
Politecnico di Torino

Nanotechnologies for ICTs

# Optimization and scale-up of electrolysers in Membrane Electrode Assembly layout for electrochemical CO2 conversion

**Master thesis**

Supervisors:

Candidate:

**Prof. Elena Maria Tresso**

**Sara Verhovez**

**Dr. Adriano Sacco**

**October 2024**

# Summary

The growing demand for sustainable energy solutions has driven the development of efficient, scalable technologies, with electrochemical CO2 conversion emerging as a key method to mitigate carbon emissions. This thesis focuses on the scale-up and optimization of electrolyzer systems for the electrochemical reduction of carbon dioxide ($CO_2$) into valuable chemicals such as carbon monoxide (CO), which serves as a crucial intermediate in the production of synthetic fuels and chemicals. Specifically, the Membrane Electrode Assembly (MEA) electrolyzer is the main focus of this research, as it holds great promise for industrial scale-up of CO2 reduction reaction ($CO_2$RR) due to its high efficiency and compact design.

The objective of the thesis is to optimize the electrolyzer setup realized with a 5 $cm^2$ MEA cell, and transpose it to a 25 $cm^2$ MEA cell setup, in order to address new challenges and limitations, and evaluate its potential for industrial applications.

The thesis begins with a comparison of MEA electrolyzers to other reactor types, demonstrating why MEA technology is superior in terms of scalability and performance. It also provides a detailed explanation of the materials and methods used in the project, including the operational parameters and setup.

The optimization process is then discussed: all the degrees of freedom in our system (such as electrodes, catalyst and membrane) are optimized, starting from the development of the ink containing the cathode catalyst, which after optimization allowed for uniform distribution of catalytic materials on the electrodes. The selection of suitable membranes and gas diffusion layers (GDLs) also played a key role in the system's performance. Sustainion® anion exchange membranes (AEMs) were chosen for their superior conductivity and stability, while the SGC 28BC GDL was found to provide an optimal balance between mechanical stability and low resistance, which is crucial for scaling up the system.

The transition from a 5 $cm^2$ to a 25 $cm^2$ electrolyzer cell introduced new challenges, particularly in terms of managing the cell potential and ensuring consistent performance. Results demonstrated that spray coating, rather than dip coating, may be exploited to provide better control over the anode's material distribution and layer thickness and enable operation of the cell at a higher current density.

In fact, a Faradaic efficiency of 97% was reached during one-hour measurement, and continuous operation was successfully maintained at a current density of 300 $mA/cm^2$ with a cell potential of 3.6 V over a 12-hour period. During this time, the Faradaic efficiency remained above 40%, demonstrating the feasibility of sustained and scalable operation.

The findings of this thesis demonstrate that with optimized materials and assembly processes, MEA electrolyzers can be scaled successfully while maintaining high efficiency. This work highlights both the promise and limitations of electrochemical $CO_2$ electrolysis technology, providing valuable insights for future studies aimed at improving stability and scaling the system for industrial applications, contributing to the development of more sustainable and renewable energy systems.

# Abstract

The growing need for sustainable energy solutions necessitates the development of efficient and scalable technologies; in particular, techniques based on electrochemical conversion are now reaching industrial potential. This thesis is based on the scale-up and optimization of electrolyzer cell systems for efficient electrochemical conversion of carbon dioxide ($CO_2$) into valuable chemicals, such as carbon monoxide (CO), a crucial intermediate in the production of synthetic fuels and chemicals.

The research begins with a series of experimental investigations conducted to optimize the electrode materials, membranes, and operational parameters of a commercial 5cm$^2$ cell, in order to identify the best possible set-up, as well as key limitations and areas for improvement. The optimization is then carried out increasing the scale of the electrolyzer cell (25 cm$^2$) to identify newfound limitations and counteract with different scaling strategies in order to improve the overall system performance.

Through the optimization efforts, it was possible to achieve comparable performance in the cell with bigger active area. In fact, it was possible to obtain comparable results to the smaller cell without efficiency loss, achieving high Faradaic efficiency (>92%) even at high current density, and continuous operation was successfully maintained at a current density of 300 mA/cm$^2$ with a cell potential of 3.6 V over a 12-hour period. During this time, the Faradaic efficiency remained above 40%, demonstrating the feasibility of sustained and scalable operation. However, some limitations were also observed, including increased cell resistance and challenges in maintaining high efficiency and stable operation continuously over a longer timeframe.

The outcome of this thesis aims to contribute to the advancement of electrochemical conversion technologies, demonstrating their potential for large-scale implementation and paving the way for more sustainable industrial processes.

# Contents

# List of Figures

# List of Tables

# Introduction

The increasing energy consumption has major implications for the environment, particularly in terms of greenhouse gas emissions and climate change. Over the past century, the concentration of atmospheric carbon dioxide ($CO_2$) has steeply risen, and rising $CO_2$ levels are widely believed to be the main cause of global climate change [1]. High amounts of $CO_2$ are released as end products from a great variety of industrial and human activities. In fact, any industrial process that contains carbonaceous fuels combustion (particularly coal, crude oil and petroleum) produces large volumes of carbon emissions [2].

The Earth system has natural processes for capturing $CO_2$, such as photosynthesis in plants, or the carbon cycle which play a crucial role in balancing and regulating its concentration in the atmosphere. However, the increase in human activities and industrial processes resulting in higher $CO_2$ emissions [3] has disrupted these cycles and led to the current state of global warming and climate change [4].

In order to handle these issues, the compelling need to transition to a more sustainable economy has risen. This urgency, intensified by a global energy crisis, has highlighted the need to not only mitigate carbon emissions but also to explore innovative ways to repurpose $CO_2$ as a valuable resource [5].

Among the various strategies developed to address this challenge, the electrochemical conversion of $CO_2$ has emerged as a particularly promising approach due to its potential to produce a wide range of value-added fuels and chemicals [6] without any revolutionary change in the platform as it can be integrated into existing energy and chemical infrastructure with minimal disruption. Moreover, by coupling this technology with renewable electricity sources (e.g., wind or solar as shown in figure 1), it could help shift industrial production towards a carbon-neutral pathway, thereby contributing to establish a neutral fossil cycle and eventually realize a carbon-neutral society. Additionally, since it uses electricity to drive the chemical reactions, this technology offers a direct path for storing intermittent renewable energy as chemical energy, effectively transform-

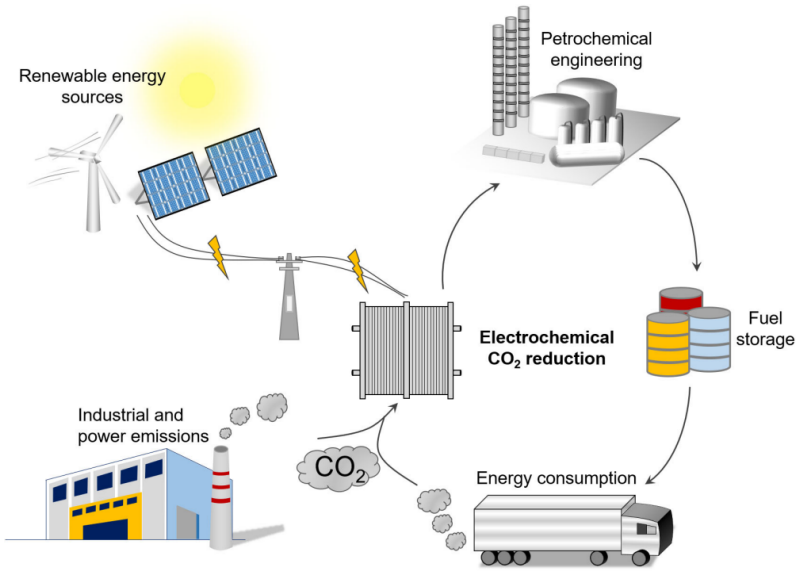


Figure 1: The schematic diagram of electrochemical conversion of $CO_2$ into fuels and chemicals using renewably sourced electricity, reproduced from [8]

ing $CO_2$ into storable and transportable forms of energy [7]. iau

Moreover, the conversion of $CO_2$ to carbon monoxide (CO) in particular is considered as the most promising reaction in the industrial market, due to its high efficiency, simpler process and optimal performances. For these specific reason, this particular electrochemical reaction has been chosen as the focus of this project.

To contribute to obtaining a circular carbon economy, however, this technology has to reach industrial standard. While laboratory-scale systems have demonstrated promising results, reaching high performance efficiency, large-scale industrial implementation of these systems is necessary to truly impact global carbon cycles and address the energy and environmental challenges we are facing today.

The objective of this thesis project is to characterize and optimize an electrolyser specifically in a Membrane Electrode Assembly (MEA) configuration, for the electrochemical conversion of CO2 to CO, by means of silver catalyst and cesium bicarbonate as electrolyte.

Once the system is optimized at a smaller scale, the setup will be scaled up to larger sizes, with further optimization required to ensure comparable performance at each stage.

The goal is to fulfill industrial requirements in both efficiency and long-term

stability, ensuring that the setup remains viable for large-scale applications and the fabrication methods are updated to yield the best possible results.

# Electrochemical $CO_2$ reduction reaction

## 2.1 Introduction

Carbon dioxide ($CO_2$) is a nonpolar linear molecule, composed of one carbon atom covalently double bonded to two oxygen atoms, making it the most oxidised form of carbon. This configurations renders the molecule chemically inert, and consequently highly stable from thermodynamics point of view.

At room temperature, this molecule exists as a colorless gas, and although it constitutes a smaller fraction of Earth's atmosphere, it is essential to many natural processes.

Its most significant role is within the carbon cycle, a dynamic and intricate system that continuously recycles and reuses carbon atoms throughout the Earth's biosphere, atmosphere, oceans, and geosphere. This cycle includes a variety of chemical processes, such as reduction/oxidation processes, where carbon atoms in compounds either gain or lose electrons.

Both geological and biological activities, including photosynthesis and respiration, depend on these transitions. The cycle is then completed when carbon is released back into the atmosphere during the respiration or decomposition of organisms.

The necessity to counteract the increase of carbon emissions has led to the development of innovative techniques for $CO_2$ capture and re-utilization that mimic the nature scheme, such as electrochemical conversion processes. However, due to the high stability of this molecule, its reduction requires significant energy input to overcome the costs associated with thermodynamical barriers. A proper catalysis is also required in order to accelerate the conversion rates.

Once these barrier are overcome, by supplying a voltage in the electrolysis process and selecting the right catalyst, a wide range of beneficial products can be

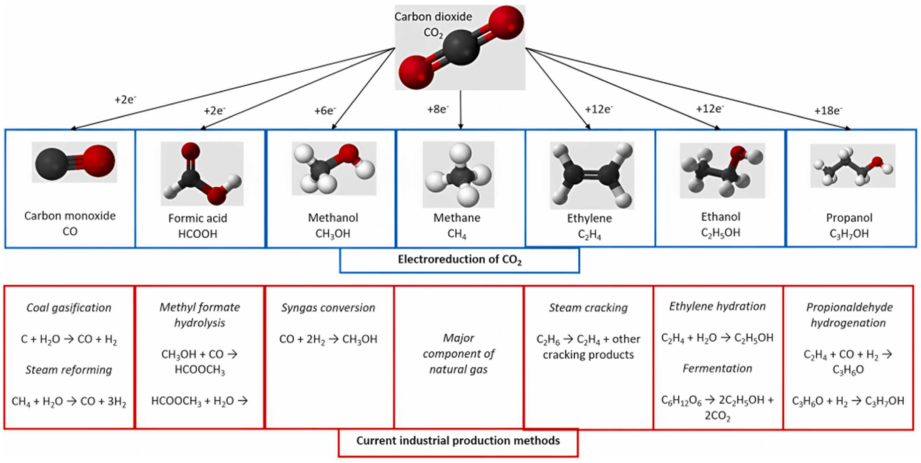


Figure 2: Products obtainable with $CO_2$RR, adapted from [9]

synthesized from $CO_2$.

## 2.2 Thermodynamical analysis of the electrochemical conversion of $CO_2$

The electrochemical $CO_2$ reduction reaction ($CO_2$RR) can be exploited to extract valuable fuels and chemicals from various stationary sources of $CO_2$, by converting it into more reduced chemical species using electrical energy.

The reaction typically involves the transfer of electrons to $CO_2$ molecules at the cathode of an electrolyzer cell under the application of an electrical current.

A great variety of reactions can be obtained with this process, each leading to the formation of specific products (shown in Figure 2), with varying reduction potentials. The main end products that can be obtained are carbon monoxide (CO), formate (HCOO-), methane ($CH_4$), ethylene ($C_2H_4$), and ethanol ($C_2H_5OH$), which are selected depending on choice of catalyst and reaction conditions. Indeed, the selectivity (i.e. the capability of convert $CO_2$ to a single product) and effectiveness of this process are enhanced by the choice of catalyst employed on the cathode.

One of the main challenges in the electrochemical reduction of $CO_2$ is the competition with the hydrogen evolution reaction (HER) in aqueous electrolytes, as both processes can occur simultaneously at the cathode and are regulated by similar reaction potentials (as shown in **Table 1**). In fact, the onset of HER can significantly reduce the efficiency of $CO_2$RR by employing electrons that could otherwise reduce $CO_2$.

Consequently, catalysts and reaction conditions should be carefully designed and optimized in order to minimize HER and maximize $CO_2$RR, improving the

| **Possible half-reactions of electrochemical $CO_2$ reduction** | **Electrode potentials (V vs SHE) at pH 7** |
|---|---|
| $2H^+ + 2e^- \; H_2$ | 0.00 |
| $CO_2$ (g) + $e^- \rightarrow$ *$COO^-$ | -1.90 |
| $CO_2$ (g) + $2H^+ + 2e^- \rightarrow$ HCOOH (l) | -0.61 |
| $CO_2$ (g) + $H_2O$ (l) + $2e^- \rightarrow HCOO^-$ (aq) + $OH^-$ | -0.43 |
| $CO_2$ (g) + $2H^+ + 2e^- \rightarrow$ CO (g) + $H_2O$ (l) | -0.53 |
| $CO_2$ (g) + $H_2O$ (l) + $2e^- \rightarrow$ CO (g) + $2OH^-$ | -0.52 |
| $CO_2$ (g) + $4H^+ + 2e^- \rightarrow$ HCHO (l) + $H_2O$ (l) | -0.48 |
| $CO_2$ (g) + $3H_2O$ (l) + $4e^- \rightarrow$ HCHO (l) + $4OH^-$ | -0.89 |
| $CO_2$ (g) + $6H^+$ (l) + $6e^- \rightarrow CH_3OH$ (l) + $H_2O$ (l) | -0.38 |
| $CO_2$ (g) + $5H_2O$ (l) + $6e^- \rightarrow CH_3OH$ (l) + $6OH^-$ | -0.81 |
| $CO_2$ (g) + $8H^+ + 8e^- \rightarrow CH_4$ (g) + $2H_2O$ (l) | -0.24 |
| $CO_2$ (g) + $6H_2O$ (l) + $8e^- \rightarrow CH_4$ (g) + $8OH^-$ | -0.25 |
| $2CO_2$ (g) + $12H^+ + 12e^- \rightarrow C_2H_4$ (g) + $4H_2O$ (l) | +0.06 |
| $2CO_2$ (g) + $8H_2O$ (l) + $12e^- \rightarrow C_2H$ (g) + $12OH^-$ | -0.34 |

Table 1: Electrochemical potentials of possible $CO_2$ reduction reactions in aqueous solutions for the production of different hydrocarbon fuels versus Standard Hydrogen Electrode (SHE) in standard conditions, adapted from [10][11].

overall system efficiency and selectivity for the desired product[12].

## 2.3 Electrolyzers

A typical electrolyzer cell for electrochemical conversion of $CO_2$ consists of three main components: the cathode (where $CO_2$ reduction occurs), the anode (where a counter-reaction like oxygen evolution takes place), and a ion exchange membrane separating the two electrodes that allows passage of ions. The $CO_2$ gas is introduced into the cell typically at the cathode either via a gas tube or dissolved in liquid.

The system design impacts several key factors, such as the cell overpotential, mass transport, stability, reaction rates, product crossover, and the overall current density. Each electrolyzer system design has several variations which come with trade-offs across the various metrics that define their performance, which may pose limitation to the development of scaled up systems for industrial applications.

We can distinguish two main categories of electrolyzers, depending on the method used for delivering the $CO_2$ at the cathode: liquid-fed and gas-fed.

In liquid-fed electrolyzers, both the cathode and anode are supplied with liquid through inlets. $CO_2$ is typically introduced either dissolved in the electrolyte or generated in situ from bicarbonate or carbonate sources.

On the other hand, gas-fed systems, where $CO_2$ is supplied directly to the

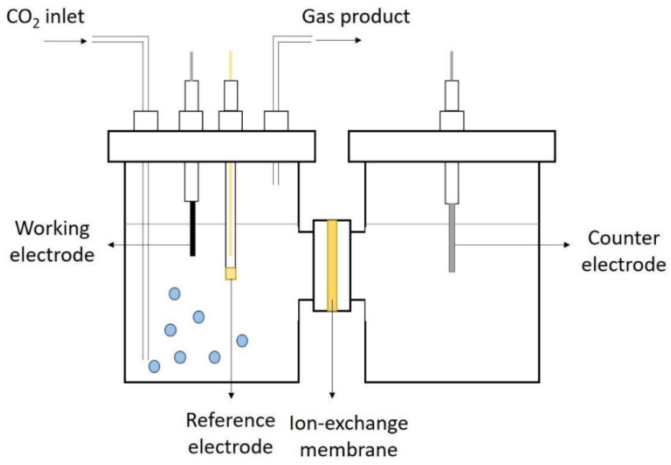


Figure 3: Schematic representation of a H-type cell, reproduced from [13].

cathode via a gas diffusion layer (GDL), have been developed to improve the productivity of electrochemical $CO_2$ conversion with respect to the liquid-fed configuration, since it greatly increases the availability of $CO_2$ at the reaction site. Gas-fed systems are generally divided into two types: the flow cell and the zero-gap cell. Although they share a similar $CO_2$ supply method and electrolyzer design configuration, the flow cell uses a liquid catholyte whereas the zero-gap does not, instead featuring a direct mechanical contact between the cathode and the membrane.

### 2.3.1 H-type cell

The H-type setup, shown in Figure 3, consists in two compartments (one anodic, and one cathodic), separated by an ion exchange membrane. During operation, $CO_2$ is continuously pumped into the electrolyte on the cathode side, where the reduction reaction occurs.

This setup is straightforward and commonly used in lab-scale experiments, as it enables high selectivity for $CO_2$ products, mostly due to the presence of the membrane that reduces cross reactions. However, despite its success in controlled laboratory settings, its industrialization still faces significant challenges.

One of the major drawbacks of this setup is given by the limited $CO_2$ solubility in the electrolyte in standard conditions. In fact, especially when increasing current density, the reaction is mass transport limited, and the amount of $CO_2$ molecules reaching the reaction site will decrease, leading to a lower reaction rate. In other words, the cell's ability to process $CO_2$ efficiently is constrained by the limited availability of $CO_2$ at the reaction site. This issue can be improved upon by acting on operational parameters, such as applying higher pressure

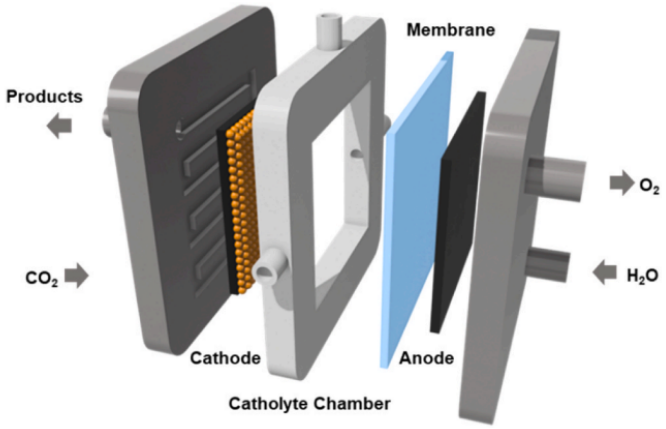


Figure 4: Schemcatic representation of a flow cell, reproduced from [17].

and lowering the temperature, as $CO_2$ solubility should increase. Even yet, the benefits are only slights, as the mass transfer of $CO_2$ from the bulk solution to the electrode surface is not greatly increased by these adjustments.

Due to the aforementioned issues, the $CO_2$ reduction partial current density is limited to around 30 mA/cm$^2$ for CO [14], and still lower than 80 mA/cm [15] in the case of other products. This limitation makes it challenging to scale up the H-type cell for industrial applications, as the current density and overall efficiency required for large-scale operations remain unattainable with this configuration in its present form.

### 2.3.2 Flow cell

The basic flow cell architecture, shown in figure 4, consists of three independent flow channels, the $CO_2$ gas channel, catholyte channel and anolyte channel. This three-phase interface has been developed to greatly improve $CO_2$ mass transfer efficiency: the gas-phase reactants and products are continuously flowed into and away from the gas flow channel, so high $CO_2$ availability can be maintained at the electrocatalyst surface of the GDE (see section 2.4.1), while the liquid products can be driven out of the reactor by the continuously flowing catholyte. A membrane is also installed between the catholyte and anolyte channels to allow ion exchange and mitigate the product crossover. The continuous flow of $CO_2$ gas over the catalyst surface ensures high $CO_2$ availability, leading to better reaction rates and product yields, as well as much higher current densities reachable with respect to the H-type cell, as shown by Yang et al.: in fact, they demonstrated that the flow cell can reach similar Faradaic efficiency at a partial CO current density ($j_{CO}$) that was 5 times higher than that of a H-type cell [16].

The flow cell design is scalable and suitable for larger-scale operations. However, there are still notable challenges that arise from this configuration, in particular due to the presence of the electrolyte.

One of the main consequences is the creation of an acidic environment right beside the membrane; while this environment enhances ion exchange, it also may extend to the cathode, consequently favouring HER and decreasing the overall efficiency of $CO_2$ reduction. This effect can be reduced by employing buffer layers in between the membrane and the electrodes to neutralize the acidity, but at the expense of a higher resistance and overpotential of the cell, resulting in a decrease of the overall energy efficiency of the system.

Additionally, the presence of the electrolyte poses significant problems in terms of stability of operation of the device. A phenomenon known as electrowetting [18], where the electric field enables the liquid to pass through the hydrophobic layer, leads to flooding of the electrode with electrolyte, thus deteriorating the access of the gaseous reactant and impairing the efficiency of the cathode [19].

This issue represents a great limitation when it comes to scaling up the reactor for industrial use. Thus, while the flow cell design offers scalability, overcoming these stability challenges is crucial for its successful application at larger scales.

### 2.3.3 Zero-gap cell

The Zero-gap cell employing a membrane electrode assembly (MEA) system represents an evolution of the previous flow cell design: as it can be seen from Figure 5, in this system there is no electrolyte layer between the GDL and ion exchange membrane, but they are directly pressed together, reducing the gap between the cathode, ion exchange membrane and anode from a renge of millimeters to only microns. As a consequence, there is no liquid electrolyte at the cathode, basically eliminating the limitations due to solubility; $CO_2$ gas is directly fed to the catalyst surface. Instead the anodic electrolyte is usually preserved.

This zero-gap structure is specifically designed to lower the ohmic impedance of the electrolyzer, while also contrasting the problem of GDL flooding. The direct contact between the membrane and electrodes also enhances the mechanical stability and overall performance of the cell: this structure in fact allows for more stable and efficient $CO_2$ conversion in the MEA device, allowing to reach much higher both faradaic and energy efficiency.

Indeed, Jeong et al. were able to employ a MEA cell to efficiently convert $CO_2$ to CO at a current density of 380 mA/cm2 and 99% FE[21].

Another significant improvement realized by MEA cells is the decrease in overpotential. As shown by Gu et al., the energy consumption of the flow cell is twice as high than that of MEA cell, since the electrolyte regeneration accounts for the major proportion [22]. Furthermore, due to the removal of the catholyte channel, the GDE directly contacts with the Ionic exchange membrane (IEM),

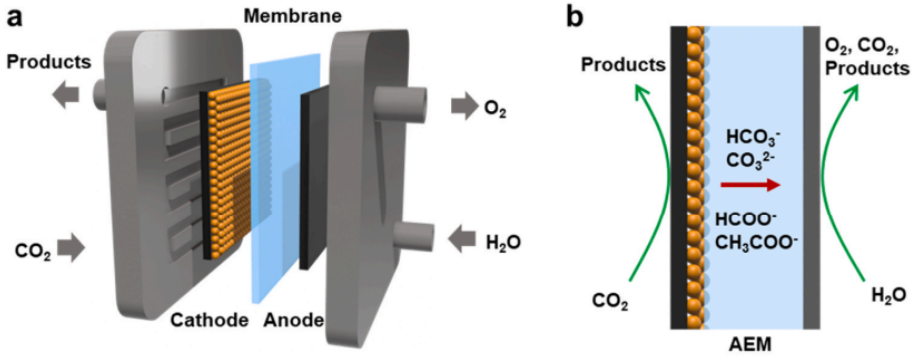


Figure 5: Schematic illustration of a zero-gap cell (a), and the dominant electrochemical reactions and CO2 crossover occurring in the same cell containing an AEM (b), reproduced from [20].

| **Industrial benchmarks for electrolysers to convert CO2 to CO** | |
|---|---|
| Electrolyzer current density | >200 mA/cm$^2$ |
| Energy efficiency | >50% |
| Faradaic efficiency | >80% |
| Full cell potential @ 300 mA/cm$_2$ | <3.0 V, better <2.5 V, ideally <2.0 V |
| Single pass conversion | >50% |
| System temperature | 60–90 °C |
| Stability | <10 µV/h |
| Cost of electricity | <0.04 USD· kW/h |

Table 2: Industrial requirements for $CO_2$ conversion to CO, adapted from [25], [26].

enhancing the transport of ions and thus largely lowering the overall cell resistance as well as improving full-cell EE [23].

Since it is significantly better than H-type cells and flow cells in terms of selectivity, current density and stability the MEA system is currently the most promising $CO_2$RR device for achieving industrial scale-up [24].

## 2.4 Performance metrics

To understand and evaluate the electrocatalyst performance towards the electrochemical $CO_2$ reduction to CO, there are certain definitions and comparison methods that need to be clarified beforehand. In fact, to be economically viable for industrialization, the reactor system setup should meet certain performance metrics (as reported in Table 2), which include current density, Faradaic efficiency (FE), energy efficiency (EE), and stability [20].

### 2.4.1 Faradaic efficiency

The faradaic efficiency (FE) is defined as the percentage of the charge related to the formation of the desired product (in this case, CO) with respect to the total charge provided to the electrode. The FE is calculated using the following equation:

$$FE = \frac{\chi nF}{Q}$$

where $\chi$ is the number of electrons transferred in the reaction (2 for $CO_2$RR to CO), n is the number of moles of CO formed during the $CO_2$RR, F is Faraday's constant (96485 C/mol) and Q is the total amount of charge passed during the reaction [27].

The FE therefore enables the understanding of the percentage and therefore amount of CO produced in the process with respect to the HER (which in our specific case is the only competitive reaction).

### 2.4.2 Current density

This is obtained by normalizing the current by either the surface area of the electrode or the electrocatalyst, as follows:

$$CD = I/A$$

usually expressed in $A/cm^2$.

This value indicates the amount of reaction occurring during the reduction to CO, and is closely related to the calculation of the faradaic efficiency (FE). Moreover, it is important especially from an industrial application point of view given that it will determine the production and operation cost of running the electrochemical setup.

Recent technoeconomic analysis have demonstrated the importance of maintaining high current densities (over hundreds of $mA/cm^2$) in order to render the $CO_2$RR practically viable [28][29][30]. These high rates are needed to ensure that the capital cost of the electrolyzer (when spread out over its operating lifetime) contributes minimally to the overall cost [22].

It is also possible to define a partial current density, referred to a single product, defined as follows:

$$J_{product} = FE_{product} \cdot CD$$

Generally, in an electrochemical system, a higher CD corresponds to a higher reactant reduction rate; higher partial CD instead indicates a higher specific product generation rate, which is therefore related to selectivity.

### 2.4.3 Overpotential

The onset potential is the minimum potential applied to the electrocatalyst for CO to be detected. The overpotential instead is the difference between the onset potential and the thermodynamic equilibrium potential of the $CO_2$RR to CO reaction. Therefore, a desirable reductive electrocatalyst should require the highest positive onset potential, while having the smallest possible overpotential [27].

### 2.4.4 Energetic efficiency

Energetic efficiency (EE) is a commonly used performance metric, generally defined as:

$$EE = \frac{E^0 \cdot (FE)}{E^0 + \eta} = \frac{E^0 \cdot (FE)}{E}$$

where $E^0$ is the reversible cell voltage, $FE$ is the Faradaic efficiency, $\eta$ is the cell overpotential, and $E = E^0 + \eta$ is the cell potential at the desired current density. In other words, the EE characterizes the efficiency of converting applied electric potential into the desired product (CO), combining the effect of losses due to non-ideal selectivity (FE) and polarization losses ($\eta$).

Due to MEA's zero-gap configuration, the ohmic losses are generally reduced with respect to other electrolyzers, enabling lower full-cell voltage and therefore higher EE.

### 2.4.5 Stability

Stability describes the variation of current density, Faradaic and energetic efficiency with time due to the deactivation of catalyst and/or degradation of the components in the cell. Better stability allows the reduction of maintenance and replacement costs, therefore playing an important role in the scale-up of the process [30].

However, this figure of merit often comes with a trade-off with respect to the previous ones: in fact many of the solutions employed in order to reach higher efficiency or current density (e.g. the use of GDE, AEM), are actually not effective from this other point of view and can hinder the stability of the system (again, e.g. due to flooding of the GDE, dehydration of AEM) [31]. In fact, the electrolyser stability still represents the main limitation to its industrialization.

## 2.5 Electrolyzer components

### 2.5.1 Electrolyte

The nature of the electrolyte, in terms of both pH and cation identity, has recently been evaluated as an important factor, which greatly affects the en-

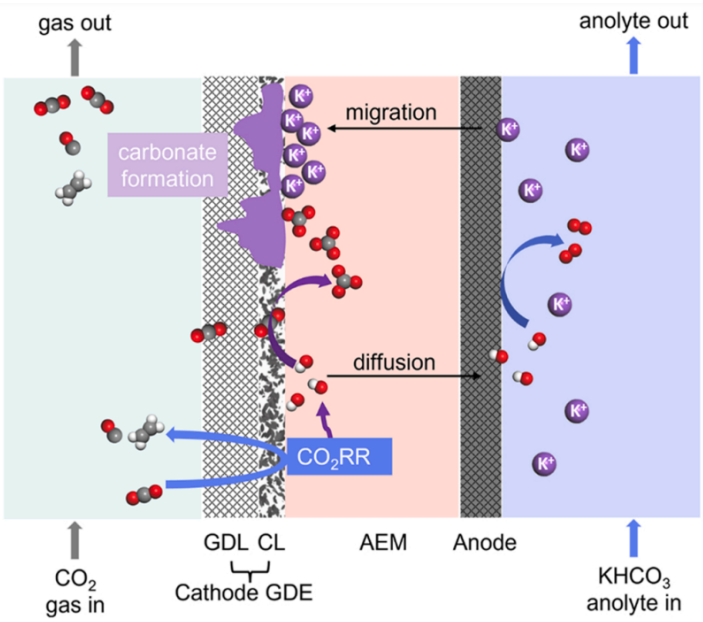


Figure 6: Schematic representation of carbonate formation process on the cathode of an MEA electrolyser, reproduced from [33]

ergy and Faradaic efficiency, and could be exploited to mitigate the previously mentioned effect of salt precipitation [32].

As cations migrate from the anode side, (bi)carbonate salts can precipitate and accumulate on the cathode side, blocking GDE pores. This phenomenon is illustrated in Figure 6. In fact, especially at high reaction rates, that involve high water consumption and high anion production, the solubility limit of the salts can be exceeded easily. This shows that both composition and concentration of the electrolyte is crucial to mitigate this issue.

The most commonly investigated electrolytes consist of either $OH^-$, $HCO_3$- or $CO_3^{2-}$ as anions and either $Li^+$, $Na^+$, $K^+$, $Rb^+$ or $Cs^+$ as cations. Table 3 lists the solubility and prices of different alkali metal salts. A high solubility can be advantageous, as it allows higher ion concentrations before salt crystallites form.

The use of (bi)carbonate electrolytes usually leads to a significant improvement in overall energy efficiency, while avoiding the losses caused by excessive $CO_2$, which is why they have great potential although potentially enhancing salt formation on the electrode [34].

(Bi)carbonate salts comprising $Cs^+$ or $Rb^+$ cations show the highest solubility but are rarely used due their high price (4–28 times higher compared to

| Alkali metal cation | OH- (M) | HCO3- (M) | Solubility in water CO32- (M) | Price $ per kg CO32- salt |
|---|---|---|---|---|
| Li+ | 5.22 | — | 0.18 | 239 |
| Na+ | 25.00 | 1.23 | 2.90 | 146 |
| K+ | 21.57 | 3.62 | 8.03 | 121 |
| Rb+ | 16.88 | 7.92 | 9.66 | 3480 |
| Cs+ | 20.01 | 10.78 | 8.01 | 546 |

Table 3: Comparison of solubility and price of various alkali metal hydroxide and (bi)carbonate salts, adapted from [35].

potassium carbonate). It was also found that $Cs^+$ containing electrolytes form smaller and more evenly distributed precipitates compared to cells using potassium containing electrolytes, resulting in a slower decrease in $CO_2$ reduction performance [35].

Significant differences are also seen in the ionic radiuses of the cations employed. Specifically the ionic radiuses of Na, K, Rb, and Cs are 102, 138, 152, and 167 pm, respectively. Cations with small ionic radiuses often show larger hydration powers (therefore, $Li^+ > Na^+ > K^+ > Rb^+ > Cs^+$) [32]. Consequently, the smaller a cation is, the smaller is its propensity to adsorb on an electrode surface.

The use of a large cation, $Cs^+$ resulted in large improvements regarding the resultant energetic (60%) and faradaic (95%) efficiencies at high current densities [36].

Most works also choose the salt concentration either for optimal electrochemical performance or for durability, depending on the scope of the study. Most publications reporting long-term tests (>100 h) use low anolyte salt concentration between 0.01–0.1 M. However, it is reported that utilizing low salt concentrations only delays the formation of precipitates in the cathode and increases cell overpotential (as it has lower conduction).

### 2.5.2 Gas Diffusion Electrode (GDE)

Gas diffusion electrodes are constituted by a substrate (the GDL) on which the catalyst is deposited, forming a catalyst layer(CL).

The GDL is made of a porous material, composed of a dense array of carbon fibers, and provides a passage for reactants as well as an electrically conductive path for current collection. It can feature a single macroporous substrate (MPS) or a double layer, which also adds a microporous layer (MPL) on one side[37].

The MPL must be hydrophobic in order to obtain optimal transport of reacting gases to the catalytic layer while also avoiding flooding or excessive drying of the crucial part of the cell. It also provides a better contact resistance between the MPS and the catalytic layer. A schematic representation of a GDE is reported in Figure 7.

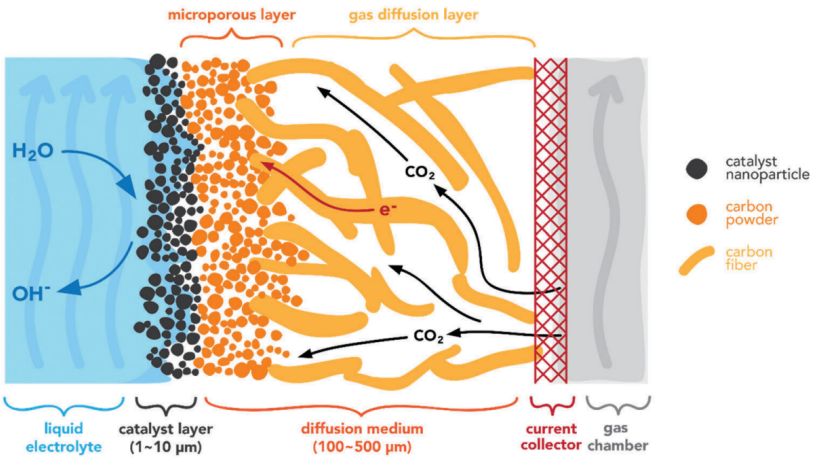


Figure 7: Schematic of a gas diffusion electrode, reproduced from [38].

The use of a GDE enables higher reaction rates and lower potential as compared to an aqueous system as it increases local $CO_2$ availability, which is still the main reactant despite $CO_2$ being supplied to the GDE from the gas phase [38].

In fact, the porosity of the GDL can help achieve high $CO_2$ concentration at the catalyst surface, and the hydrophobicity ensures $CO_2$ availability by preventing electrolytes from flooding the pores of the GDL. The most important characteristic of GDE is that it creates a triple-phase interface ($CO_2$, catalyst, electrolyte), where the $CO_2$ gas is initially dissolved into the thin electrolyte layer surrounding the catalysts and then reduced to different products. The triple-phase interface plays the dominant role in shortening the $CO_2$ diffusion length, allowing CO2 to react in the form of gas rather than firstly being dissolved in aqueous solutions [39]. Moreover, the use of GDE provides possibility to operate electrolyzers (especially zero-gap) at industrial current densities.

Despite the benefits of using a GDE, there are still some challenges that affects its performance. For instance, when using a carbon-based GDL, the electrowetting phenomenon can threaten the system stability when GDL flooding occurs. If a large amount of hydrophobic polymer (therefore overcoming the flooding challenge) is added into the GDL, the electrical conductivity decreases, and the cell resistance increases. Furthermore, salt precipitate can build-up during long operation which can block the GDL, limiting the $CO_2$ reaction.

### 2.5.3 Membrane

IEMs represent the key components of an electrolyzer. They are typically thin polymeric films containing fixed charged groups, which block selected types of ions depending on their overall charge through electrostatic repulsion and allow the passage of other types. They can be classified into: cationic exchange

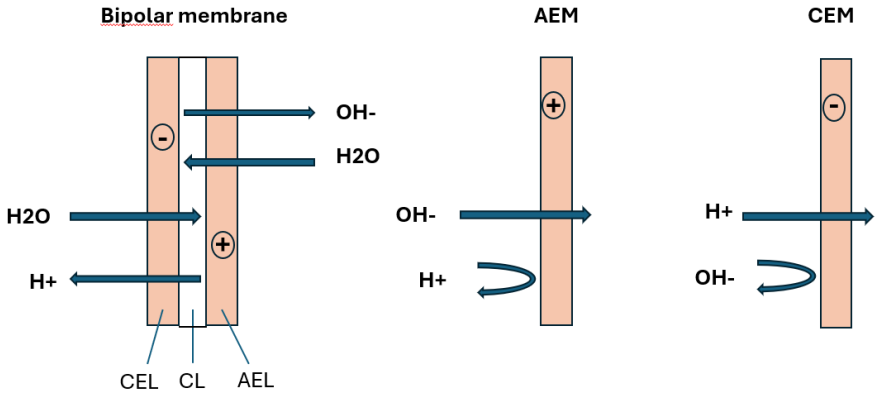


Figure 8: Schematic representation of different membrane types: BPM (reverse bias), AEM, CEM.

membrane (CEM), anion exchange membrane (AEM) and bipolar membrane (BPM). Schematic representations of these membrane types are reported in Figure 8.

The CEM contains negative functional groups, which allow cations to pass through while blocking anions. Specifically, CEMs are penetrable to protons (or positive charges) due to low internal resistance and high conductivity, while simultaneously preventing the passage of substrate or oxygen from the anode to the cathode compartments. Hence, they are often referred to as PEMs (Proton Exchange Membranes). These membranes, on the other hand, have as main disadvantages their high cost, in addition to low ion selectivity, and the creation of an acidic environment that could extend to the electrodes, risking to favour HER and impairing both energy and Faradaic efficiency of the system.

Conversely, the AEM blocks cations while allowing anions to pass through; this avoids high local $H^+$ concentration and therefore minimizing undesired HER on the cathode. This membrane leads to better performances in alkaline systems, mainly due to cation cross-over from the anode to the cathode, as $CO_2$ reacts with OH- forming $CO_3^{2-}$ and $HCO_3^-$ ions. However, this also results in precipitate formation in the cathode GDE, which is a major limitation in these types of systems. In fact, the precipitate salt will reduce active surface area on the electrode, hindering flow of $CO_2$ to the catalyst and therefore decreasing reaction efficiency.

Finally, BPMs are composed of two ionomer layers: a cationic exchange layer (CEL), containing fixed negative charges, and an anionic exchange layer(AEL), containing positive fixed charges. In between them usually can be found a neutral catalyst layer (CL)[40].

BPMs have two operating modes in electrochemical systems: forward and re-

verse bias.

In forward bias, cations and anions are transported respectively towards the AEL and CEL interface, where they recombine. In reverse bias, electric fields and catalytic effects in the CL layer cause the breakdown of polarizable species into cations and anions which are then transported to the respective layer.

The ability for BPMs to control and maintain different local chemical environments and drive the dissociation or formation of chemical species with an applied voltage makes BPMs particularly viable for electrochemical applications. A drawback of using BPMs is the increased cell voltage, rooted in the additional interface between the two layers (and possible water dissociation catalyst) and in the voltage needed to facilitate water dissociation at that same interface [41].

AEMs are currently favored over CEMs for zero-gap electrolyzers, as the alkaline to neutral environment is favorable for $CO_2$ reduction selectivity over the hydrogen evolution reaction, hence why they were the preferred option for the setup used in this project. However, their optimization remains critical as it requires balancing multiple trade-offs: as an example, a higher ion exchange increases water uptake (WU) and consequently membrane swelling, thus reducing ionic resistance but also permselectivity of the membrane. In fact, reduced permselectivity results in unwanted cation crossover from the anode to the cathode. Hence, the design of the polymer structure and arrangement of cationic groups in the membrane play an important part in overcoming these trade-offs [42].

Moreover, the membrane should be mechanically stable and resistant to dehydration in order to be used for long term operation of the system.

### 2.5.4 Catalyst

As mentioned before, the catalyst deposited on the cathode is crucial for minimizing the energy needed for specific reactions by reducing the activation energy, therefore selecting the type of reaction and product to be obtained [25].

Various materials have been tested for electrochemical conversion, and it has been shown that specific metals can produce specific products: as an example Sn or Bi are the best for producing formate, and Cu-based catalysts are for $C_2H_4$ [43]. For CO, the main catalysts used are Ag or Au, where Ag shows generally higher stability than Au[44].

Additionally, the anodic catalyst is also quite important, as it has to be chosen and designed to favour the complementary process (typically the electrochemical oxygen evolution reaction, OER). The catalysts used are generally Ir, Ni or Pt. While Ni is the most stable material in alkaline solutions, Ir is the most popular choice in $CO_2$ electrolyzer cells, despite not being nearly as stable in alkaline environment. In fact, it was demonstrated that due to the neutralization of the recirculated anolyte, anode catalysts must be stable under near-neutral OER conditions, hence why Ir results to be more stable, while Ni instead is only

applicable in cells where the alkaline conditions at the anode were continuously ensured [41]. However, the worldwide supply of iridium is limited, and so more valid alternatives to iridium need to be investigated to allow $CO_2$ electrolysis to grow at industrial level.

Recently, a variety of electrocatalysts for the GDE cathode has been used for the $CO_2$ reduction to CO, mostly noble and non-noble metals.

In the case of noble metals, in the past decade, gold (Au) and silver (Ag) have been the two most commonly explored metals for the electro-conversion of CO2 to CO.

Au has been studied extensively as the ideal catalyst for this process, due to its optimal binding energy for the key intermediate of COOH, which is essential in the reduction process to CO. This also translates into an overall lower overpotential and highest catalytic activity and FE among the catalysts. However, the rarity and high cost of Au severely limit its actual application, especially at industrial level. Accordingly, many recent studies are conducted to address this issue by optimizing and further improving the cost efficiency of Au by methods such as using nanoparticles (NPs), but the effects of reducing particle size on overall performance are still being investigated.

Alternatively, Ag is another highly investigated potential electrocatalyst, in fact being the second ideal electrocatalyst for this process, again due to similar reasons to that of Au, where it has the second optimal binding for the COOH intermediate [45]. Theoretically, its required overpotential is even lower than that of Au but at the cost of current density. It is also much cheaper than Au, despite still being an expensive alternative. However, when exploring methods to reduce the cost such as decreasing particles size, it was demonstrated that the use of Ag NPs significantly improve both electrocatalytic performance and product, hence why Ag has been shown to be a cheaper and more popular alternative [46].

Other non-noble metal alternatives that are more available and environmentally friendly, such as zinc (Zn) and bismuth (Bi) are also being studied, but there is still a fundamental lack of understanding of the underlying effect they have on cell performance.

### 2.5.5 End plates

The metallic end plates have several functions: they form the electrodes which are in contact with the catalyst layers and are mostly responsible for the reactants supply to the cell active area, and for the proper outlet of the products through the channels. The three commonly adopted flow patterns are the serpentine, parallel, and interdigitated designs, as shown in Figure 9; each having a different mass transport mechanism mainly dependent on pressure drop on the flow channels. Therefore, this pattern must be always optimized towards the targeted application in the employed setup [47].

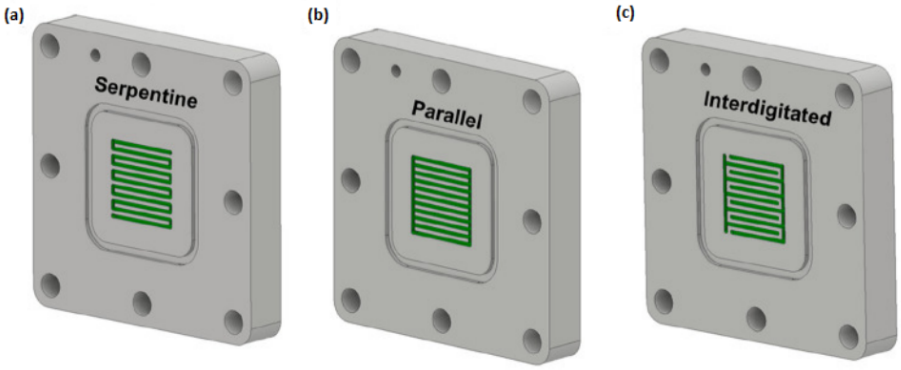


Figure 9: Different shapes of flow channels carved in the end plates (serpentine, parallel and interdigitated, respectively), adapted from [48].

In particular, the serpentine-shaped flow channel has been demonstrated to outperform the other shapes in terms of partial current density, resistance to flooding and catalyst utilization [48], hence why in this setup the serpentine flow field is also used.

When scaling up devices to larger areas, however, the implementation of multi-path systems will become essential to avoid excessive pressure drops in devices. In $CO_2$RR research, it remains crucial to find ways to completely avoid issues such as flooding and salt formation altogether, exploring several different strategies (pulsing, water flushing, etc.) [49].

# Materials and methods

In this chapter, all the methods relative to the fabrication of the electrodes and the analysis of the cell performance will be detailed.

## 3.1 Methods for electrode fabrication

### 3.1.1 Spray-coating

Spray coating is a deposition technique that involves the atomization of a liquid solution into fine droplets, which are then sprayed onto the surface of a substrate. This technique uses a spray nozzle to break the ink containing the material to be deposited into a mist of tiny particles, which evenly cover the target surface delimited by a mask to select a specific area.

The model used is a Nadetech Ultrasonic spray coater (shown in Figure 10), which contains a piezoelectric oscillator that produces standing waves, causing the droplets to fall from wave tops.

This machine allows to obtain fairly uniform deposition of catalyst on the electrode, for surface areas up to 100 $cm^2$.

The critical part of this technique is represented by the ink optimization: in fact, all the components (catalyst, binder and solvent) and the ratio between them have to be chosen specifically in order to deposit the desired amount of product uniformly and minimizing the losses. Spray coating was used to fabricate the cathode used in this project.

### 3.1.2 Sputtering

Sputtering is a physical deposition technique from vapour phase precursor (PVD), which employs a vacuum chamber containing two electrodes: one with the target (cathode, representing the material to be deposited), and the other with the substrate on which the material has to be deposited (anode, which has to be conductive). When a potential between the two electrodes is applied, plasma

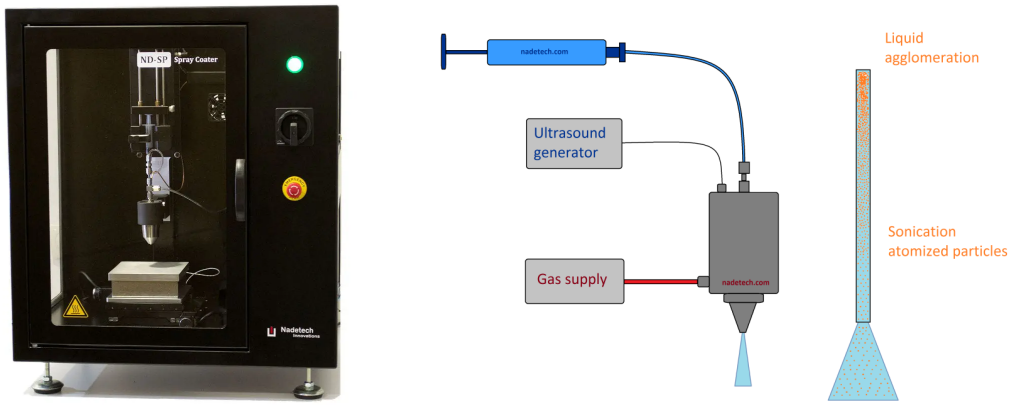


Figure 10: Ultrasonic Spray Coater from Nadetech on the left, and a schematic representing its working principle on the right.

(high reactive ions) form in between the gas: Ar+ ions are accelerated and bombard the target, which ejects atoms of the material to be deposited, which in turn will travel towards the other electrode and attach to the substrate.

This technique allows to obtain highly uniform results, but it is not viable for scaled systems. Large-scale sputter-deposition of hard protective coatings has not been prevalent as the large dimensions of the industrial targets posed an enormous technological challenge: only relatively low power (and plasma) densities could be achieved, resulting ultimately in poor performance of such coatings [50].

Sputtering was used to fabricate the cathode used in this project, alternatively to spray coating.

### 3.1.3 Dip coating

Dip coating is a method used to apply a thin, uniform layer on a surface by soaking the substrate in a liquid coating solution and then withdrawing it at a controlled speed. The process involves immersing the object, allowing it to interact with the liquid, and then slowly pulling it out.

Dip coating is widely used due to its simplicity, ensuring an even coating over complex surfaces, allowing for precise control of thickness, and being cost-effective. This technique was used to fabricate the anode used in this project.

## 3.2 Electrochemical characterization

In this section all the electrochemical techniques used to analyse the performance of the setup will be listed and described, as well as the parameters investigated


Figure 11: The Biologic potentiostat (on the left) used to power the cell and carry electrochemical measurements, along with the Inficon Micro-GC Fusion (on the right).

to define the cell.

During this thesis project, three key techniques - Electrochemical Impedance Spectroscopy (EIS), Chronopotentiometry (CP), and Linear Sweep Voltammetry (LSV) - were employed to investigate the electrochemical properties and performance of the cell. These techniques were employed by using a potentiostat paired up with a booster (Bio-Logic HCP-803, shown in Figure 11) in order to amplify the current and voltage ranges of measurement up to 80 A and 5 V.

### 3.2.1 Electrochemical Impedance Spectroscopy (EIS)

EIS is a technique used to study the frequency response of electrochemical systems. By applying a small alternating current (AC) signal and measuring the resultant voltage response, EIS enables the evaluation of resistance, capacitance, and diffusion-related properties of the system under study over a wide range of frequencies. This method is particularly useful for characterizing charge-transfer processes, electrolyte resistance, and diffusion layers, gaining insights into both kinetics and mass transport phenomena. EIS data are usually represented in Nyquist or Bode plots, which are analyzed to extract equivalent circuit parameters for the system under study.

Analyzing a MEA configuration yields a Nyquist curve that is similar to the simplified Randles cell's: the equivalent circuit is comprised of a solution resistance and a parallel between a double layer capacitance and a charge transfer (or polarization resistance). From this curve it is possible to identify the resistance of the cell and predict the behaviour of the overpotential, as well as obtain information about the electrochemical regime and properties of the sys-

tem [51]. This curve also indicates that at this frequency region the reaction rate is controlled by charge transfer phenomena and not by mass transport [52].

### 3.2.2 Chronopotentiometry (CP)

CP is a galvanostatic electrochemical analysis method: it involves the application of a constant current to the cell while monitoring the resulting potential over time. This technique is especially useful for studying material stability, resistance, and eventually reveal the breakdown of electrodes and changes in the materials' structure or setup due to prolonged current exposure[53].

For each configuration, CP measurements of 1 hour were carried out to track the cell overpotential during operation, while simultaneously analyzing the gaseous products by using gaschromatography (GC) technique.

### 3.2.3 Gaschromatography (GC)

GC is an advanced analytical technique employed for the separation, identification and quantification of volatile and semi-volatile compounds within a complex mixture.

As the components of a gaseous mixture reach the inlet of a GC system, they move through a separation column undergoing a number of processes involving interaction with a stationary phase inside the column, which cause different components to exit and reach the detector at different times [54]. This separation process results in the generation of a Gaussian-shaped peak for each component of the mixture; from the integration of these curves, parameters relative to the detected gas - such as its concentration - can be extracted. A micro-gascromatographer (Inficon Micro GC Fusion® Gas Analyzer) was also used during CP measurements.

### 3.2.4 Linear Sweep Voltammetry (LSV)

LSV is a dynamic electrochemical technique where the potential of the working electrode is linearly swept at a defined rate, while the resulting current is recorded. This method is employed to probe redox processes, reaction kinetics, and the electrochemical window of the system. LSV is mostly useful for gaining insight into peak currents and potentials, which are indicative of reaction rates and thermodynamics. This technique will be particularly important for the scale up of the system, in order to visualize how the cell overpotential would change when increasing current density.

## 3.3 Experimental setup

In this section, the chosen cell setup will be described, as well as the assembling of its components and the operative parameters.

Focusing on the electrochemical conversion of $CO_2$ to CO, the MEA configuration was chosen as the most optimal for a scale up. In particular, bicarbonate is chosen as the electrolyte, as it has been widely used to achieve selective $CO_2$ conversion at high current densities [55], despite being more incline to carbonate formation.

When selecting the right type of catalyst for CO, at the cathode the resulting reaction will be:

$$CO_2 + 2H^+ + 2e^- \rightarrow CO + 2H_2O$$

while at the anode it will be:

$$2H_2O \rightarrow O_2 + 4H^+ + 4e^-$$

The cell components are:

- flow plates,
- membrane (AEM)
- anode, realized by dip coating and calcinating a layer of IrO2 on a Ti substrate
- cathode, a carbon paper on which Ag catalyst was deposited using spray coating technique
- gaskets, PTFE masks inserted on both sides, with different thickness to ensure right amount of pressure on both cathode and anode
- electrolyte(anolyte), a bicarbonate solution.

Despite being the most promising system for industrial applications, the zero-gap cell still faces challenges (as shown in Table 4) that have to be overcome by carefully tuning each parameter. Moreover, MEA is a complex system: its performance is highly dependent on the contributions of many components, including cathode reaction, anode reaction, ion transportation, and electrode-membrane interface exchanges, phenomena that are affected by each component, and often interact with each other.

In this section the effect of each component on these key phenomena in the MEA system will be investigated, and I will explain the rationale behind selecting specific materials and configurations for the setup used in this project, aiming to illustrate how the chosen setup addresses the main challenges of $CO_2$ electrolysis.

### 3.3.1 Membranes

In this work, Sustainion® X37-50 Grade RT (an imidazolium functionalized polystyrene membrane) provided by Dioxide Materials was mostly utilized, but other anionic membranes - such as PiperION® - were tested throughout the project based on the aforementioned characteristics.

| **Shortcomings** | **Implications** | **Potential solutions** |
|---|---|---|
| Flooding | closure of CO2 transfer pores | - adjusting GDE water uptake via ion-exchange capacity and GDE thickness<br>- controlling cathode GDE hydrophobicity via PTFE content |
| | | - separating cathode GDE from - liquid media by a gas passing section |
| CO2 crossover to the anode side | losing CO2 in the cathode | - using a tandem design consisting of SOEC and MEA |
| | re-emission of CO2 with O2 in the anode | - using acidic media with a CAL to enrich K+ at the catalyst surface |
| Product concentration | necessitates a costly separation stage | using a carrier gas (such as N2) to collect high-purity products |
| Carbonate formation on the cathode GDE | Blockage of CO2 transport.<br>Reducing reaction efficiency.<br>Unstable CO2RR operation. | considering a regenerative cell voltage, lower than the operational voltage to lower carbonate ions concentrations on the cathode and mitigate salt formation |
| Cation crossover from anode to cathode when using alkaline solution in anode | precipitation on the cathode GDE due to the reaction with crossover cation, CO2, and electrogenerated OH | using pure water as anolyte and periodically infusing the cathode with alkali cation-containing solutions (e.g., 0.5 M KOH) |
| High voltage loss | reducing energy efficiency | designing no electrolyte cell, using AEM and improving membrane-catalyst interface |

Table 4: Adapted from [24]

### 3.3.2 Anodes

Dip coating was used to fabricate the anode used in this project. In particular, the $IrO_2$ anodic catalyst was deposited onto a commercial Ti felt trough the following steps (also shown in Figure 12):

- firstly the Ti felt is wet etched in HCl, in order to remove impurities, then washed thoroughly with deionized water and let dry on a hot plate
- the Ti felt is immersed in a solution of $IrCl_4$ dispersed in ethanol, and pulled up
- the coated felt is then let dry on a hot plate for a few minutes
- the felt is then calcinated for a few minutes at 450 °C
- the felt is let out, and let cool down, before repeating the last three steps (dip coating, drying, calcinating) until the catalyst has reached the desired loading (which in this case is 2.5 mg/cm$^2$).

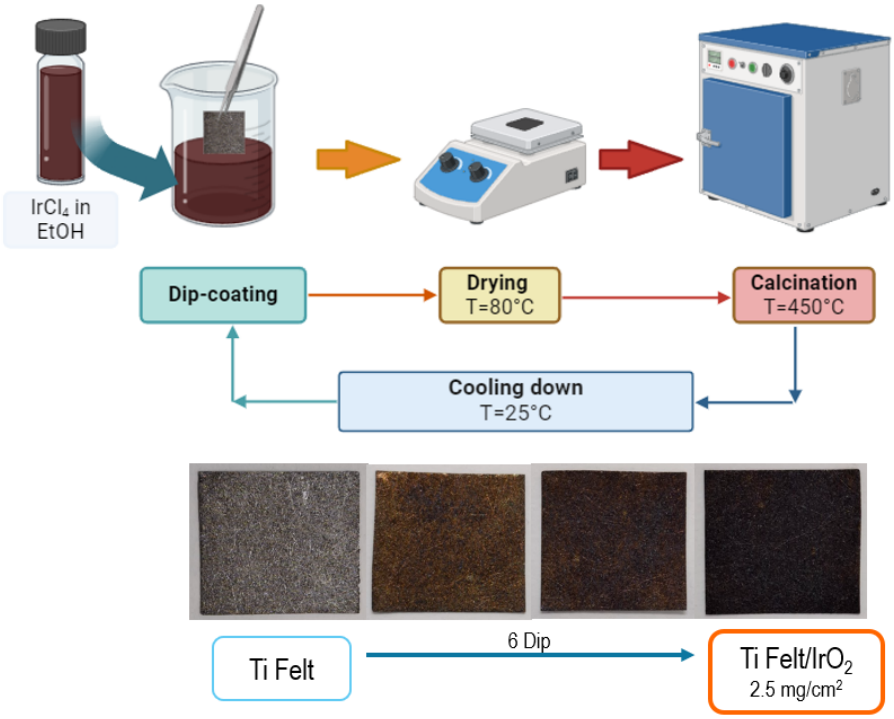


Figure 12: Schematic representation of the anode manufacturing technique steps, along with the resulting Ti felt.

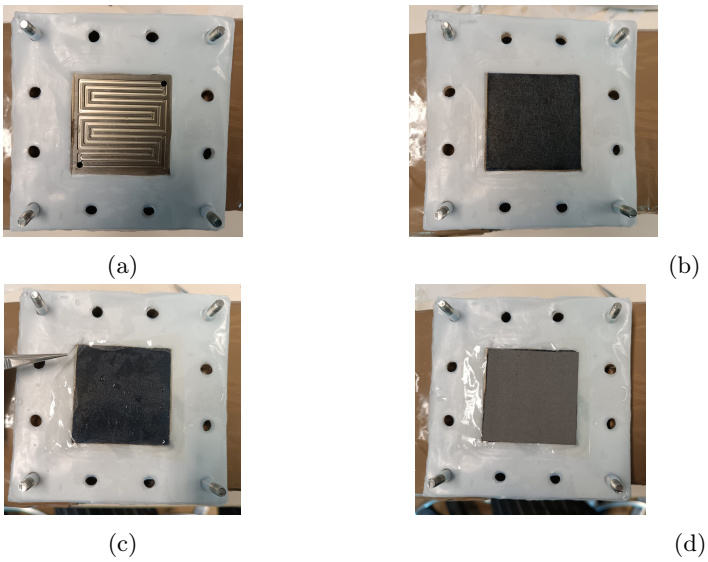

Figure 13: Assembling process for the MEA electrolyzer cell. At first the gaskets for the anode are positioned (a), the anode is added in the space in the middle (b), the membrane is put on top (c) and finally the cathode along with the gasket (d). The cell can now be closed with the end metallic plates.

### 3.3.3 Cathodes

Due to the aforementioned properties (section 2.5.4) and previous studies, in this thesis project it was chosen to use as catalyst Ag NPs. To fabricate the GDE, silver nanoparticles ($d_{avg} < 150$ nm, Sigma-Aldrich) were dispersed in a 1:3 isopropanol/water mixture, together with 5wt% ionomer binder, matching the membrane used at the start of our project (in this case, Sustainion® XA-9). A ultrasonic bath was used to disperse the Ag nanoparticles in the solvent for around 45 minutes before spray coating on a 5 $cm^2$ substrate. The main components, such as catalyst, binder and solvent were varied in order to optimize the recipe and catalyst deposition on the cathode substrate.

### 3.3.4 Electrolytes

For the scope of this thesis, it was chosen to use cesium bicarbonate ($CsHCO_3$) 0.1 M as electrolyte, in order to reach optimal conditions and maintain lower salt precipitation phenomena. However, in the optics of a further scale up and industrialization, more accessible and cost-effective electrolytes will have to be investigated.

Figure 14: The peristaltic pump used in this setup to supply electrolyte to the cell.

### 3.3.5 Assembly and operational parameters

The cell components are assembled and the cell is closed in a crossed way, first applying a torque of 2 N/m, then 4 N/m. PTFE gaskets are also inserted around the electrodes, in order to define the pressure exerted on them, which in turn affects the interface between catalyst and the other cell components (see figure 13. A gasket of 285 $\mu$m is inserted in the anode compartment, while the gasket thickness on the cathode side is generally varied depending on the substrate employed. Generally, a gasket of 150um was paired with a commercial Sigracet (SGC) 28BC substrate.

The electrolyte is circulating at the anode using a pump at 24.55 mL/min. At the cathode instead $CO_2$ is fed at 100 mL/min controlled by a multi-channels peristaltic pump (BT100-L by LongerPump, showed in Figure 14), and is humidified before entering the cell, in order to improve the overall stability and durability of the setup. In fact, operating the cell without gas humidification can lead to membrane dry-out, failure and increase of salt formation on the cathode. The flux is regulated via a mass flow controller (EL-Flow Select, Bronkhorst) directly connected to the $CO_2$ gas cylinder. Gas traps are also placed right after the mass flow and at the end of the circuit, just before the GC connection, in order to prevent any unwanted liquid from the setup from entering these sensitive devices, ensuring the integrity and accuracy of the gas measurements.

The final closed cell is shown in Figure 16, while the setup is represented in Figure 15.

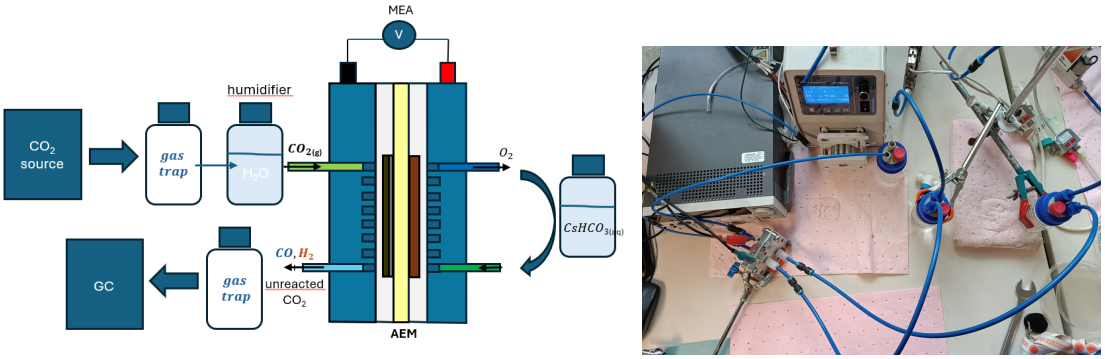


Figure 15: Schematic representation of the setup used during the measurements.

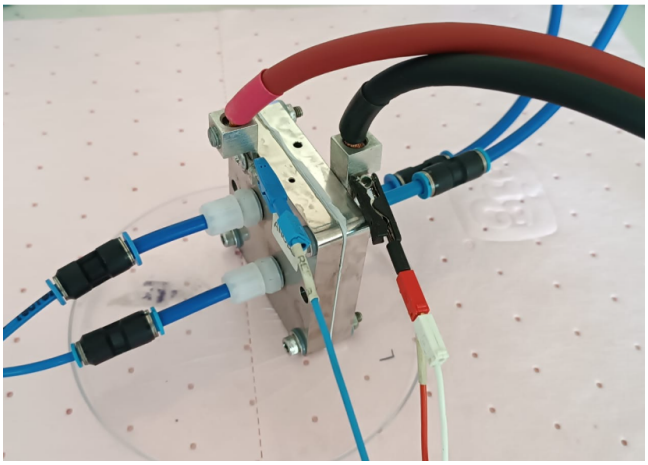

Figure 16: Assembled 5cm$^2$ MEA cell.

# Optimization of 5cm$^2$ cell setup

In this section, the optimization of the parameters of our system is described, starting from optimization of the ink components for the catalyst deposition up to the cathode optimization. The final results of this process are then shown and the system is tested in terms of efficiency, cell voltage, current density and finally, stability.

## 4.1 Cathode loading

Firstly, the amount of catalyst to be deposited on the cathode electrode was investigated.

In view of a scale up of the system, a lower amount of loading (measured in mg/cm$^2$) is preferred as it would resolve in a more cost-effective solution.

In fact, results showed that lower loading (in this case 0.5mg/cm$^2$) allowed to obtain the best results in terms of both Faradaic efficiency and cell overpotential. It achieved high electrochemical performance (reaching an $FE_{CO}$ of 92%) and cell potential $< 4$ V, making it the most promising candidate among the other higher-loaded electrodes.

## 4.2 Optimization of spray-coating ink recipe

### 4.2.1 Solvent

The ratio of nanoparticles with respect to solvent has to be optimized in order to obtain a good quality dispersion that will result in a more uniform deposition and smaller product loss from the spray coating process. Different ratios were investigated in order to obtain a loading of 0.5mg/cm$^2$: the amount of NPs (6 mg) was fixed and the volume of solvent was varied instead. Electrodes realized with three different inks (with NPs/solvent ratios equal to 3:1, 3:2 and 3:4) were produced the best ink recipe was selected based on electrochemical activity, percentage of product loss in the spray coating process, uniformity of

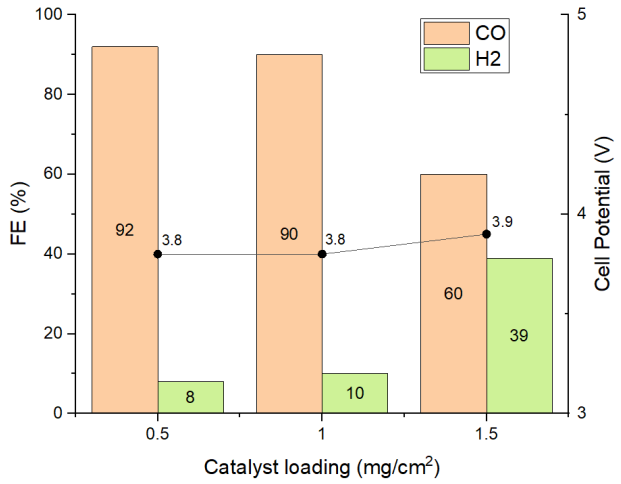


Figure 17: CP measurements of samples with different cathode loading at 300 mA/cm$^2$.

dispersion and deposition, and reliability of results obtained during repeated measurements.

In the following are reported the ratios investigated:

- 3:1 ratio (corresponding to 6 mg of Ag NPs dispersed into 2 mL in total of solvent) resulted in non uniform deposition and too diverging repeated measurements, causing problems of reliability.
- 3:2 ratio (meaning 6 mg of Ag NPs dispersed into 4 mL in total of solvent) gave both the best electrochemical performance, dispersion and less amount of product loss (40%); in fact it was chosen as the ideal ratio.
- 3:4 ratio (meaning 6 mg of Ag NPs dispersed into 8 mL in total of solvent), while a bigger amount of solvent should guarantee a more optimal dispersion, it resulted in a bigger product loss (60%) and longer deposition time via spray coating.

### 4.2.2 Binder

To proceed with the ink optimization, different commercial binders (5% cat. wt) were tested in the fabrication of a 0.5 mg/cm$^2$ Ag NPs loaded electrode:

- Sustainion® XA-9 Alkalyne ionomer (5% in ethanol)
- PiperION® Anion Exchange Dispersion 5% wt.
- Nafion™ 117 (5% solution)
- Fumion FAA-3-SOLUT-10 Anion Exchange Ionomer (8-12 wt%)

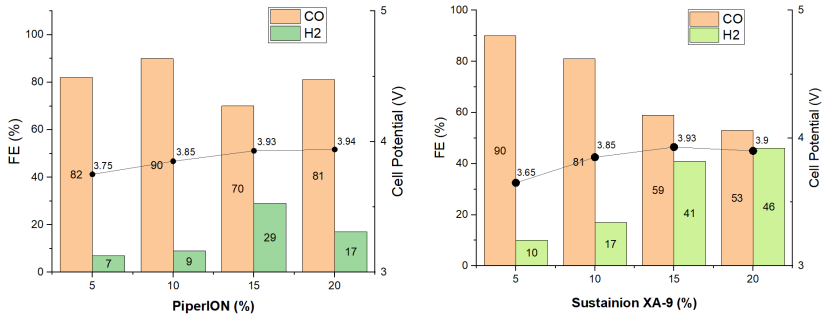


Figure 18: Comparison of different percentage of PiperION® binder(on the left) and percentage of Sustainion XA-9 binder (on the right).

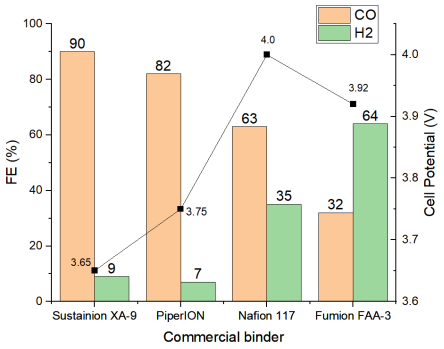


Figure 19: Comparison of different commercial binders.

Results of electrochemical characterization are showed in Figure 18a. While the Nafion and Fumion binders lead to a subpar performance, Sustainion® binder was the best performing one, and it was therefore investigated further in terms of concentration in the ink. However both performance and conductivity of the cell was reported to decrease drastically when increasing its amount inside the solvent (figure 18b). Moreover, despite its lower performance when coupled with Sustainion® membrane, the use of PiperION® binder has been investigated further when matched with PiperION® AEM, as it could enhance the ion conductivity properties of the membrane. In Section 4.4 this will be explored thoroughly.

## 4.3 Cathode substrate

Next, the effect of the GDL on the cell performance was studied. Five different GDLs were investigated (Sigracet28BC, SGC22BB, SGC39BB, Toray60-MPL, FreudenbergH23C6) and analyzed in terms of Faradaic efficiency and resistance.

The five carbon papers all differed in thickness, porosity and other properties,

showed in Table 5. These properties impact greatly on the final cell performance: presence of an MPL, the porosity and crack formation on the GDL (or GDE) all have a great influence on the electrolyte management, hence affecting the rate and selectivity of CO2RR. In particular, the presence of cracks on the MPL (as in Figure 20) has been correlated to a better water management, which is highly beneficial for the $CO_2$ reaction [56].

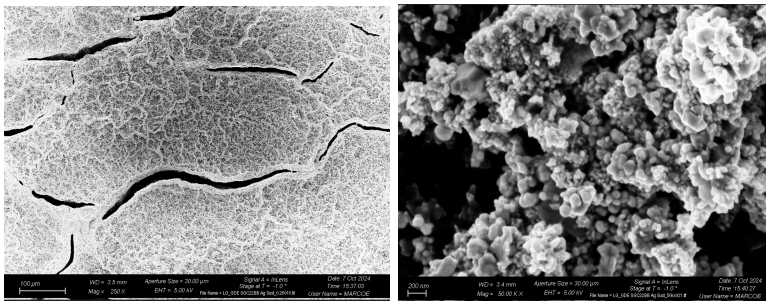

Figure 20: SEM images of the GDL of a substrate (SGC 28BC) with catalyst layer (Ag NPs), in which the cracks on the GDL are visible

Some important properties, such as the gas permeation and the electrical resistance of these GDLs, are highly dependent on the measurement conditions and the experimental setup, as they vary notably upon compressing the GDL.

The optimal compression ratio might depend on the thickness and structure of each GDL. The compression selected for each was found by modifying the cathode gasket in our setup depending on the thickness of the GDL at issue, and by verifying which compression optimized the CO production. Indeed, a higher compression resulted in a lower resistance, but also hindered the $CO_2$ conversion resulting in a slightly lower FE.

It is also to be noted that all the carbon papers analyzed contain a MPL, which is reported to be essential for avoiding flooding and favouring of HER instead of desired reduction process[56].

From the results (showed in Figure 21), the best performing GDLs are the SGC 28BC and the TO60-MPL. However, although differing very little in resistance (found by means of EIS measurements), some distinctions were found in the cell overpotential, with the thicker GDLs (SGC 39BB, TO60-MPL) generally leading to a higher cell voltage. The Freudenberg H23C6 instead showed much subpar performance compared to the others, which may be correlated to its MPL being the thinnest out of all and being made up of spaghetti-like fibers, which may have an effect on the GDL's wetting properties.

The SGC 28BC therefore exhibited the best trade-off, leading to both high FE and lower cell potential, which will be critical when scaling up the device since the current density requirements ($300 mA/cm^2$) should be satisfied. Also note that generally thicker GDLs are reported to be more mechanically stable in long

| Manufact. | Type | Thickness/µm | | PTFE in | PTFE in | Porosity | Compressib. |
|---|---|---|---|---|---|---|---|
| | | Total | MPL | CFL(%) | MPL(%) | (%) | (%) |
| Sigracet | 39BB | 315 | 93±18 | 5 | 20-25 | n/a | 13 |
| Sigracet | 28BC | 235 | 74±15 | 5 | 23 | 76 | 15 |
| Toray | 060-MPL | 250 | 93±8 | 8-9 | 33-35 | 78 | 10 |
| Freudenberg | H23C6 | 250 | 37±7 | n/a | n/a | 61 | 20 |
| Sigracet | 22BB | 215 | 74±15 | 5 | 20-25 | 72 | 20 |

Table 5: Most important technical parameters of the GDLs investigated, adapted from [56], [57]

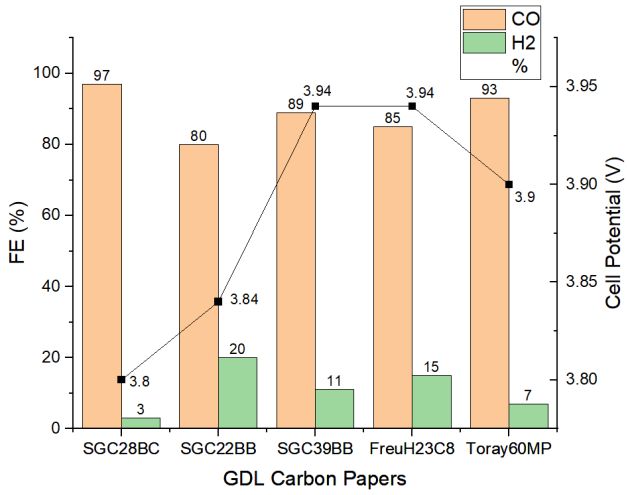


Figure 21: FE and cell overpotential obtained during 1 hour-long CP measurements, operating at j = 300 mA/cm$^2$.

term measurements[56], but it was not possible to verify this claim during this project.

## 4.4 Membrane

Sustainion®'s AEMs have become a benchmark in this field and are utilized in many recent studies [58]. Despite the extensive use of Sustainion® AEMs in literature, they are generally unstable at a temperature above 60 °C over longer timeframes (particularly in less than fully hydrating conditions) and allow $CO_2$ product crossover to the anode during operation.

Because of its higher ultimate stress when compared to other AEMs, the PiperION® membrane (a poly(aryl piperidinium)-based AEM provided by Versogen™) exhibits better wet/dry cycling and overall mechnical stability, which makes it a

| Membrane | Thickness ($\mu$m) | Young's Modulus (MPa) | Elongation at Break (%) | IEC (meq/g) | Water uptake (wt%) | Conductivity (mS/cm, OH-, 80 °C) |
|---|---|---|---|---|---|---|
| **PiperION** | 20-80 | 30-50 | 20-100 | ∼2.35 | 50 | ∼150 |
| **Sustainion x37-50 Grade RT** | 50 | 60 | 30 | ∼2.52 | 80 | ∼140 |

Table 6: Reported mechanical and conductive properties of Sustainion® and PiperION® AEMs used in this project, adapted from [60].

promising candidate for longer operation of MEA [42]. Moreover, they have been reported to achieve notable performance both in terms of partial current density (>1.0 A/cm$^2$) and maintaining high conversion [59].

For the aforementioned reasons, PiperION®membranes with different thicknesses (20, 40, 60, 80 $\mu$m) were tested, along with their different activation methods, which are the following:

- KOH 1M
- KOH 1M, then $KHCO_3$ 1M
- $CsHCO_3$ 1M
- $NaCO_2$ 0.1 M, then $CsHCO_3$ 0.1M

These activation methods were tested onto a 60um PiperION® membrane: the results are reported in Figure 22.

Since the electical conductivity of a membrane is a property intrinsic to the membrane material itself, as well as dependent on thickness, membranes of similar thickness should exhibit comparable electrochemical behavior, and thinner membranes should reduce the overall cell resistance. However, despite most PiperION® membranes generally being thinner than Sustainion, EIS measurements showed that they introduced significantly higher cell resistance than them. This was corroborated by the fact that PiperION® membranes exhibited much higher cell overpotentials, making it difficult to operate them at current densities above 100 mA/cm$^2$, with subpar performance even when operable. In fact, the 80 µm PiperION® membrane could not be operated at all due to excessive overpotential, even at lower current densities.

Initial LSV tests of membranes activated with $CsHCO_3$, the preferred activation method for this application, revealed that only the 20 µm membrane could be operated at a current of 1.5 A (corresponding to a current density of 300 mA/cm$^2$). The 20 µm membrane also demonstrated the best performance in terms of Faradaic efficiency (FE) and cell potential at 100 mA/cm$^2$, but at higher current densities, it caused short-circuiting, while instead the thicker membranes showed higher resistance and therefore higher cell potential as expected, but also slightly lower FE. This introduces the first trade-off in optimiz-

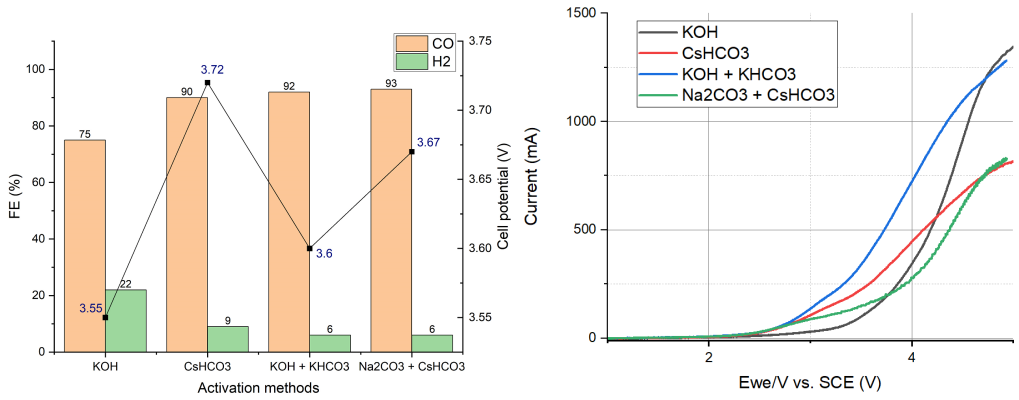


Figure 22: Comparison of activation methods for a 60 $\mu$m PiperION® membrane, through CP measurements at 100 mA/cm$^2$ (on the left) and LSV measurements (on the right).

ing AEMs: while a thinner membrane is preferred to reduce series resistance and achieve higher current densities, it should also be mechanically robust to withstand the stresses of prolonged operation.

Since the low current density represents a big limitation, another activation method was tried. After immersing the membranes in a 1M KOH bath for a few hours, the three membrane thicknesses were tested first at 100 mA/cm$^2$, then at 300 mA/cm$^2$.

The 40 µm membrane (which is similar in thickness to the Sustainion) showed the best performance and stability, reaching almost 90% of FE and much lower cell potential with respect to the other thicknesses (see Figure 23). However, in general, when increasing current density the products drastically decreased, with only the 40 µm thickness staying above 50%. Moreover, although it was possible to operate them at 300 mA/cm$^2$, the cell potential resulted well over 4V, which is not sustainable in long term operation as it could lead to faster degradation of the anode.

This high resistance is most likely due the polymer chemistry of PiperION® being quite a bit different than Sustainion membrane. While Sustainion membranes have a higher degree of functionalization and employ a crosslinking method in order to avoid solubility and obtain a mechanically stable membrane without compromising the final ion exchange capacity aspect. PiperION® membranes, on the other hand, have a predefined degree of functionalization and no crosslinking which would result in a lower ion exchange capacity (IEC), as shown in Table 6.

$HCO_2$- and $CO_3^{2-}$ were identified as majority charge carriers responsible for the ion conduction through the AEM, due to the rapid formation of HCO3- and $CO_3^{2-}$ from $OH^-$ in a $CO_2$ rich environment [61]. This observation suggests that

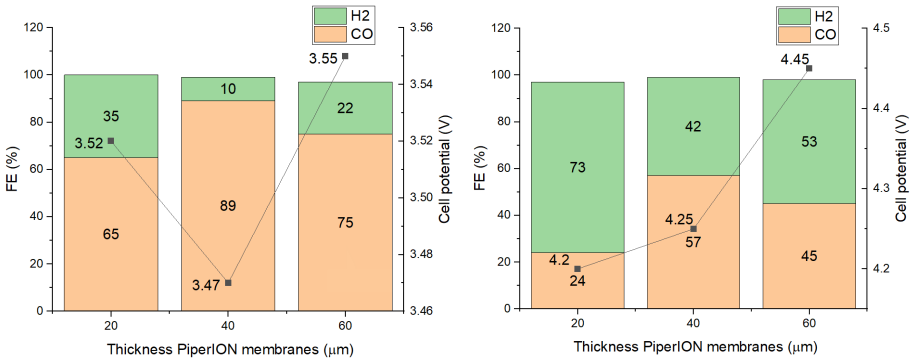


Figure 23: CP measurements of PiperION®membranes activated in KOH 1M, on the left at 100 mA/cm$^2$, and on the right at 300 mA/cm$^2$.

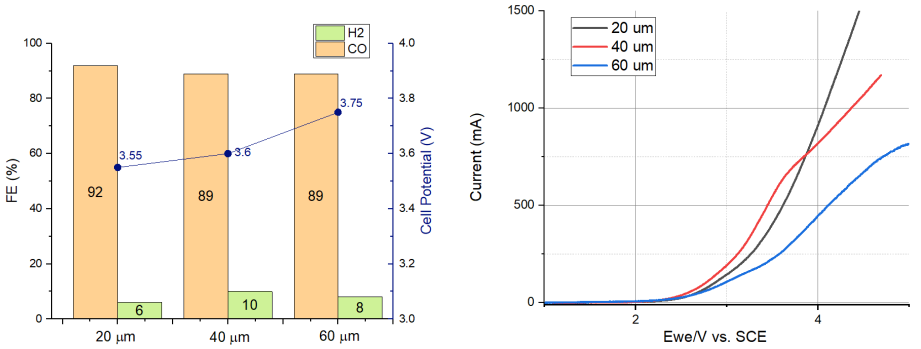


Figure 24: Comparison of different thicknesses of PiperION® membranes activated in $CsHCO_3$, through CP measurements at 100 mA/cm$^2$ (on the left) and LSV measurements (on the right).

a membrane with high carbonate/bicarbonate conductivity is a prerequisite for high current density alkalyne $CO_2$RR electrolyzers.

Since the chemistry of the membrane is not related to transfer of hydroxyls, but transfer of carbonates or bicarbonates, PiperION® membranes would have significantly lower transfer rate for bicarbonates' ions, which would result in a higher resistance.

This aspect could also be related to water uptake properties as it was also demonstrated that AEMs having low water uptake show lower net water flux through the AEM (from the anode to the cathode) in comparison to membranes having higher water uptake, due to the fact that the latter swell more, therefore allowing lower resistance for water to transport across the AEM [60].

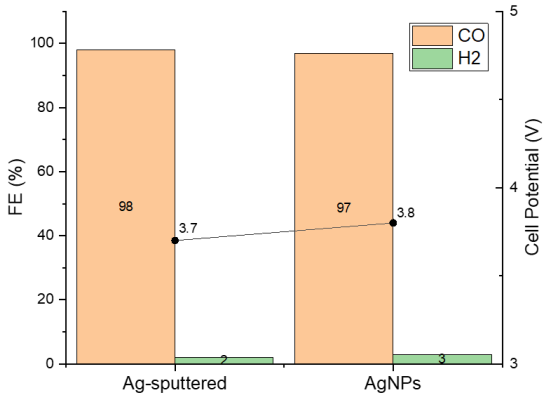


Figure 25: Comparison of the optimized low-loaded 0.5 mg/cm$^2$ AgNPs electrode at j = 300 mA/cm$^2$ with an Ag sputtered (300 s 50 mA) electrode, with same working parameters.

## 4.5 Stability test

The optimized setup, composed by:

- on the cathode: SGC 28BC GDL, Ag NPs catalyst (with loading 0.5 mg/cm$^2$), obtained with the optimized ink recipe;
- on the cathode: Ti felt, catalyst $IrO_2$ (with loading 2.5 mg/cm$^2$)
- Sustainion x37-RT AEM;

was compared in terms of electrochemical activity to a reference setup containing an Ag sputtered (200 s 50 mA) electrode, maintaining the same working/cell parameters. The two setups showed comparable results at 300 mA/cm$^2$ (Figure 25), meaning the optimization carried out in the previous sections was successful.

This setup was then tested with a long term CP measurement (lasting over 12 hours) in order to assess its stability and determine the timeline over which salt formation begins to impact the sustained operation of the cell.

The results are shown in Figure 26. In fact, operation of the cell was degraded, as after 6 hours the FE was already halved, while the potential progressively increased, reaching 4.5 V at the end of the experiment.

## 4.6 Final consideration

The optimization of the 5 cm$^2$ cell setup demonstrated significant improvements in the system's efficiency, scalability, and stability. By systematically adjusting

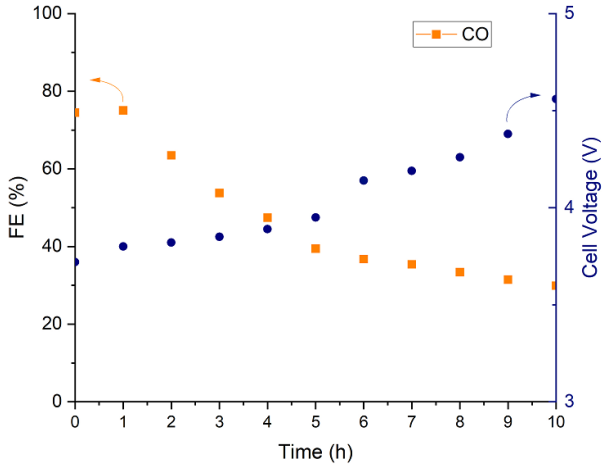


Figure 26: FE and cell potential behaviour over longer operation (>10h) at 300mA/cm$^2$

critical parameters, from the catalyst loading to the optimization of the spray-coating ink recipe and cathode substrate, a well-rounded solution was achieved that enhances both electrochemical performance and operational reliability.

In particular, the selection of a lower catalyst loading (0.5 mg/cm$^2$) proved to be an effective strategy for reducing costs while maintaining high Faradaic efficiency and low overpotential. The choice of Sustainion XA-9 as the binder further solidified the optimization by providing superior performance and conductivity, though its percentage must be carefully controlled to avoid negative impacts.

Additionally, the study of the GDLs revealed the importance of choosing the right substrate in ensuring high efficiency and low resistance: the SGC 28BC GDL emerged as the optimal choice, balancing mechanical stability and electrochemical performance, which will be essential for future scaling of the device.

Despite these advances and improvements in the setup, the long-term stability of the system remains a key limitation: while the setup sustained operation for over 12 hours, a good performance for both FE and cell potential was maintained only for around 6 hours before degradation.

# Optimization of 25cm$^2$ cell setup

## 5.1 Operational parameter optimization

When scaling up the device area, it is important to maintain the previously established parameters as closely as possible and assess whether there are significant changes in the cell's behavior.

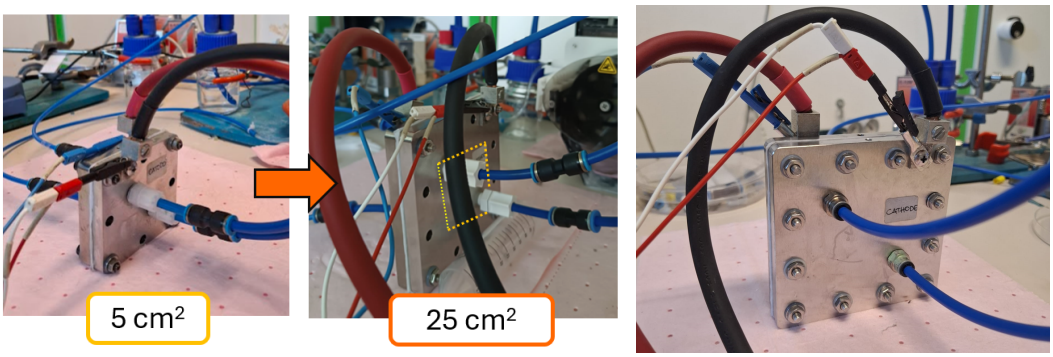


Figure 27: Transition from an MEA Electrolyzer with active area of 5 cm$^2$ to one with 25 cm$^2$. On the right, the completely assembled 25 cm$^2$ cell.

One of the primary challenges in scaling up is managing the cell potential. As the active area increases, the total current required to operate the cell will also rise, leading to a corresponding increase in cell voltage. To address this, new strategies will need to be implemented to reduce resistance, enabling operation of the cell at the same current density as before.

Firstly the impact of key operational parameters -such as $CO_2$ flow rate, electrolyte flow rate, and cathode compression - was investigated. An electrolyte flow rate of 75 RPM was chosen, while the $CO_2$ flow was maintained as 100 ml/min. Finally, LSV measurements with different cathode compression, ob-

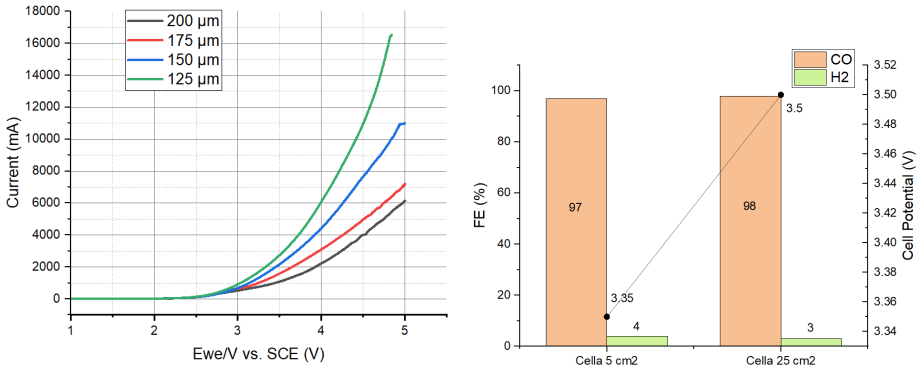


Figure 28: On the left: LSV measurements of different cathode compression (obtained by changing gasket thickness) on the 25 $cm^2$ cell. On the right: comparison of Ag sputtered cathode onto 5$cm^2$ and 25 $cm^2$, with optimized working parameters.

tained by varying the gasket thickness in the cathodic compartment from 125 $\mu$m to 200 $\mu$m, was carried out. The results of this screening, reported in Figure 28, are mostly in agreement with expectations, as a thicker gasket introduces a higher series resistance, and therefore would result in a higher cell voltage during operation. For this reason, a gasket thickness of 125 $\mu$m was chosen, in order to minimize this resistance. The anode gasket thickness instead was left unchanged.

The operation of the cell using these parameters was then tested at 100 mA/$cm^2$ and compared to the same setup on a 5 $cm^2$ cell, using a sputtered electrode (Ag NPs). The result is shown in Figure 28: in fact, performance in terms of FE are maintained even on the scaled up electrolyzer, although tan increase in cell potential is also registered. This result proves that the optimization of the working parameters was successful.

## 5.2 Optimization of spray-coating ink recipe

After setting the operational parameters, a new spray coating ink recipe has been formulated and optimized. Following the previous ones, the new recipes maintain as solvent three parts of $H_2O$ and one part of IPA. However, two recipes differing in the solvent volume were realized and tested:

- one with 6 mL total volume of solvent (1.5 mL IPA; 4.5 mL $H_2O$)
- one with 8 mL total volume of solvent (2 mL IPA; 6 mL $H_2O$)

The recipe that ensured the best performance and minor product loss during the spray coating process was the one with 6 mL of solvent: this ink recipe will therefore be used for all the electrodes with an increased area of 25 $cm^2$. The spray-coated electrode was then tested with a CP measurement at 100 mA/$cm^2$:

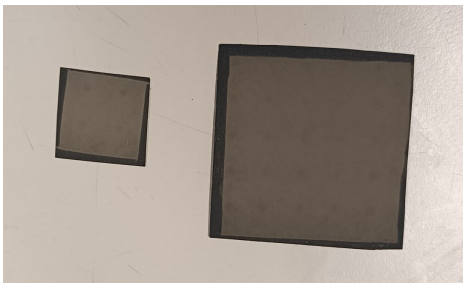

Figure 29: Comparison of two cathodes of sizes 5 $cm^2$ and 25 $cm^2$, obtained via spray-coating deposition of Ag NPs.

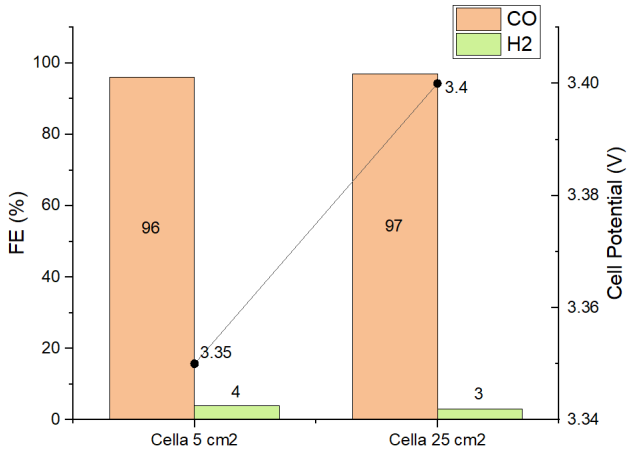


Figure 30: Comparison of spray-coated cathode (with optimized recipe) onto 5 $cm^2$ and 25 $cm^2$ setup at 100 $mA/cm^2$.

the results are much similar to those obtained with the same setup in a 5 $cm^2$ cell, although with an increase in cell potential (shown in Figure 30).

## 5.3 Anode manufacturing technique

Scaling up the components of the cell also presents some challenges in the fabrication of the anode. Indeed, while dip coating technique remains suitable for small-scale applications, it encounters significant limitations when applied to larger systems. Managing the anode during dip coating becomes more complex, often resulting in uneven material distribution and consequently less homogeneous coating, which can negatively impact the performance of the scaled-up electrolyzer. Spray coating, on the other hand, provides better control over layer thickness and uniformity, ensuring a more consistent and scalable anode surface, as well as better reproducibility of the samples.

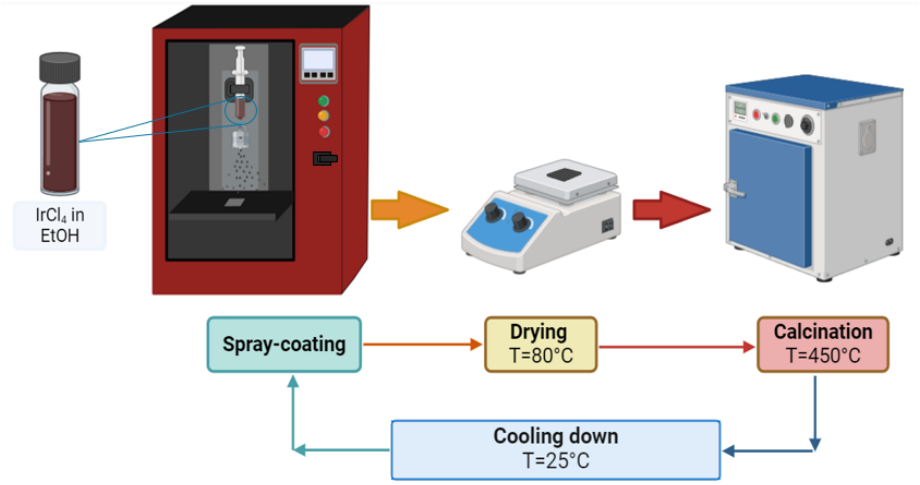


Figure 31: Schematic representation of the spray-coated anode manufacturing technique steps.

Figure 32: Comparison of a dip coated Ti felt anode (on the left) with a spray coated one (in the middle) and a commercial Ti felt (on the right).

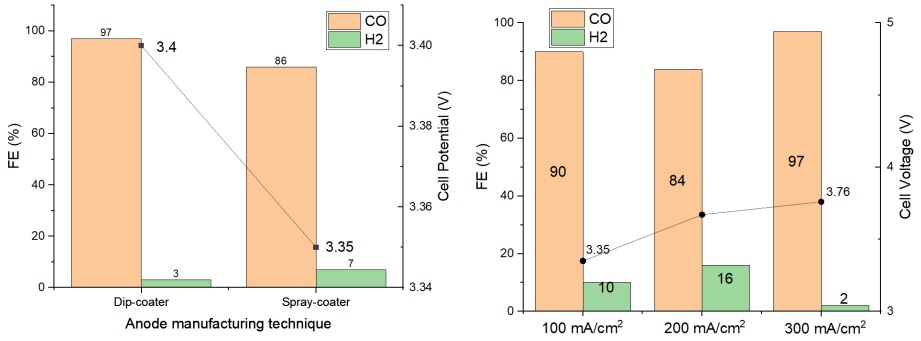


Figure 33: Performance of setup comprising spray-coated anode, first compared to the dip-coated one at 100 mA/cm$^2$, then operated at progressively higher current densities.

To evaluate its potential for large-scale applications, the performance of an anode produced through spray coating was investigated and compared to a dip-coated anode, in order to determine if it could be a viable alternative for scaling up the system. The anode maintained the same loading and properties as the dip-coated one, varying only in the deposition process (whose steps are showed in Figure 31). A comparison of the resulting Ti felt with a dip-coated and a commercial one is shown in Figure 32.

While the setup with the spray coated anode performed worse at 100 mA/cm$^2$, in terms of FE, with respect to the dip-coated anode; the spray-coated anode allowed to operate the cell at 300 mA/cm$^2$ without exceeding 4V (Figure 33).

The optimized setup comprising the spray-coated anode was then tested at different current densities, up to 300 mA/cm$^2$, achieving high electrochemical performance: an FE of 97% was registered and maintained for an hour measurement, along with a cell potential of 3.75 V. The same measurement was repeated obtaining quite good results, although with a slightly lower FE, but also much lower cell potential, which theorethically could enable operation of this setup at higher current densities.

These results determine that the transition to the 25 cm$^2$ cell was a success, as performances comparable to the smaller cell were obtained (Figure 30).

## 5.4 Stability test

The final setup, transposed onto the 25 cm$^2$ and optimized, was then tested with a long term CP measurement (>12 hours) in order to assess its stability and durability. The result is reported in Figure 35.

The FE remained above 50% for the first few hours and stayed over 40% for the duration of the experiment. Although there was a noticeable decline after

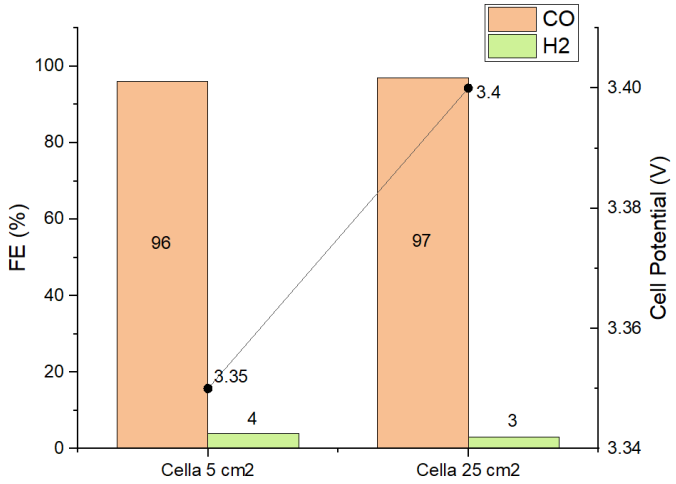


Figure 34: Performance of same setup (containing a low-loaded SGC 28BC) on 5 $cm^2$ and 25 $cm^2$ electrolyzer.

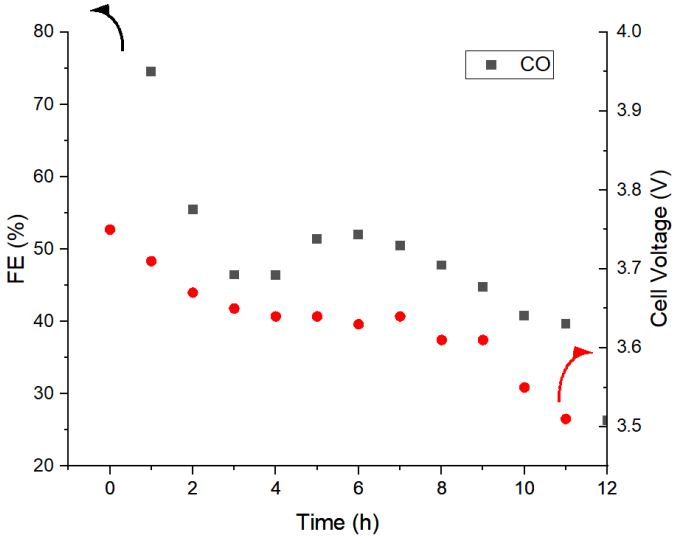


Figure 35: FE and potential behaviour of the 25 $cm^2$ setup reported over longer operation (>10h) at 300 $mA/cm^2$.

around 3 hours, likely due to a reduction in single-pass conversion (as confirmed by a mass flow reader positioned at the cathode outlet), this outcome is still significant. In fact, for the first few hours a single pass conversion of almost 40% was reached (meaning almost 40% of the $CO_2$ was effectively converted), although this value then decreased rapidly, ending the measurement at less than 10%. Moreover, curiously the cell voltage kept decreasing throughout the measurement, reaching only 3.5 V at the end.

Overall, these results highlight the system's ability to maintain a good level of efficiency and a relatively low operating voltage over an extended period, making it a promising result for future improvements and scalability.

## 5.5 Final considerations

The transition from a 5 $cm^2$ to a 25 $cm^2$ electrolyzer cell marks an important step as the start of scaling up process of the system, and the obtained results are encouraging in many respects. After the optimization and switch to a spray-coating technique for the anode fabrication, the larger cell maintained comparable performance to the smaller setup at the same current density, demonstrating the feasibility of scaling up without substantial losses in efficiency.

However, these optimizations must be further refined, as higher current densities generally still led to an overall drop in efficiency. Moreover, the long-term stability of the system at higher current densities (which is crucial for future industrial applications) still features a large area of improvement, as shown by the long-term operation measurement.

# Conclusions

The comprehensive optimization and scaling of the electrolyzer from an active area of 5 $cm^2$ to 25 $cm^2$ was executed successfully, thereby substantiating the effectiveness of the methodologies proposed for larger applications in electrochemical systems.

The use of low-loaded AgNP catalysts (0.5 $mg/cm^2$) successfully reduced material costs without compromising Faradaic efficiency or overpotential. A systematic approach was adopted in the optimization of the setup, focusing separately on all the components in order to obtain the best possible performance.

In the pursuit of maintaining the operational integrity of the scaled-up cell, a meticulous assessment of various operational parameters was undertaken, ensuring that the performance of the larger electrolyzer was not compromised when compared to its smaller counterpart. Critical parameters -including the electrolyte flow rate, $CO_2$ flow rate, and cathode compression- were optimized to achieve the desired outcomes.

The transition from the dip-coating technique, which is generally suitable for smaller-scale applications, to the spray-coating technique for the anode manufacturing represented a significant advancement in this study. Although the spray-coated anode exhibited a slightly lower FE at 100 $mA/cm^2$ compared to its dip-coated counterpart, it nonetheless proved to be more robust and capable of sustaining performance under higher current densities, successfully operating at 300 $mA/cm^2$ without exceeding a cell voltage of 4 V. This characteristic adaptability of the spray-coated anode underscores its potential suitability for large-scale applications, thereby enhancing the scalability of the electrolyzer design.

Moreover, the performance evaluation of the spray-coated anode in conjunction with the optimized cathode demonstrated promising results, achieving a FE of 97% at a current density of 300 $mA/cm^2$, which is comparable to the performance metrics observed in the original 5 $cm^2$ setup. Continuous and stable

operation was also achieved for 12 hours, with FE above 40%. This findings serve to reinforce the notion that operational consistency can be maintained even in the face of significant increases in cell size, thereby supporting the scalability of the electrolyzer system.

In summary, the successful transition to a 25 $cm^2$ cell configuration achieved during this project, coupled with the optimization of operational parameters and manufacturing techniques for the components, provides compelling evidence for the potential of these enhancements to be effectively integrated into larger-scale electrolyzers. However, several limitations still persist, such as the system's long-term stability, performance at higher current densities, and membrane resistance require further investigation. Future research should focus on optimizing membrane chemistry, refining fabrication techniques for both anodes and cathodes, and developing methods to mitigate by-product and carbonate formation to achieve more stable, efficient, and scalable electrolyzer systems, compliant with requirements for industrialization. These improvements will be critical for advancing the commercial viability of $CO_2$ conversion technologies.

# References


[1] Kelvin O Yoro and Michael O Daramola. "CO2 emission sources, greenhouse gases, and the global warming effect". In: *Advances in carbon capture*. Elsevier, 2020, pp. 3–28 (cit. on p. 9).

[2] Leonel J. R. Nunes. "The Rising Threat of Atmospheric CO2: A Review on the Causes, Impacts, and Mitigation Strategies". In: *Environments* 10.4 (2023). ISSN: 2076-3298. DOI: 10.3390/environments10040066 (cit. on p. 9).

[3] Maria Silvia Muylaert de Araujo, Christiano Pires de Campos, and Luiz Pinguelli Rosa. "GHG historical contribution by sectors, sustainable development and equity". In: *Renewable and Sustainable Energy Reviews* 11.5 (2007), pp. 988–997. ISSN: 1364-0321. DOI: https://doi.org/10.1016/j.rser.2005.07.001 (cit. on p. 9).

[4] Gadi Rothenberg. "A realistic look at CO2 emissions, climate change and the role of sustainable chemistry". In: *Sustainable Chemistry for Climate Action* 2 (2023), p. 100012. ISSN: 2772-8269. DOI: https://doi.org/10.1016/j.scca.2023.100012 (cit. on p. 9).

[5] Latifah M. Alsarhan, Alhanouf S. Alayyar, Naif B. Alqahtani, and Nezar H. Khdary. "Circular Carbon Economy (CCE): A Way to Invest CO2 and Protect the Environment, a Review". In: *Sustainability* 13.21 (2021). ISSN: 2071-1050. DOI: 10.3390/su132111625 (cit. on p. 9).

[6] Chike George Okoye-Chine, Kabir Otun, Nothando Shiba, Charles Rashama, Samson Nnaemeka Ugwu, Helen Onyeaka, and Chinedu T. Okeke. "Conversion of carbon dioxide into fuels—A review". In: *Journal of CO2 Utilization* 62 (2022), p. 102099. ISSN: 2212-9820. DOI: https://doi.org/10.1016/j.jcou.2022.102099 (cit. on p. 9).

[7] Rosa M. Cuéllar-Franca and Adisa Azapagic. "Carbon capture, storage and utilisation technologies: A critical analysis and comparison of their life cycle environmental impacts". In: *Journal of CO2 Utilization* 9 (2015), pp. 82–102. ISSN: 2212-9820. DOI: https://doi.org/10.1016/j.jcou.2014.12.001. URL: https://www.sciencedirect.com/science/article/pii/S2212982014000626 (cit. on p. 10).

[8] Yueli Quan, Jiexin Zhu, and Gengfeng Zheng. "Electrocatalytic Reactions for Converting CO2 to Value-Added Products". In: *Small Science* 1.10 (2021), p. 2100043. DOI: https://doi.org/10.1002/smsc.202100043 (cit. on p. 10).

[9] Grazia Leonzio, Anna Hankin, and Nilay Shah. "CO2 electrochemical reduction: A state-of-the-art review with economic and environmental anal-

yses". In: *Chemical Engineering Research and Design* 208 (2024), pp. 934–955. ISSN: 0263-8762. DOI: https://doi.org/10.1016/j.cherd.2024.07.014 (cit. on p. 13).

[10] Wenjun Zhang, Yi Hu, Lianbo Ma, Guoyin Zhu, Yanrong Wang, Xiaolan Xue, Renpeng Chen, Songyuan Yang, and Zhong Jin. "Progress and Perspective of Electrocatalytic CO2 Reduction for Renewable Carbonaceous Fuels and Chemicals". In: *Advanced Science* 5.1 (2018), p. 1700275. DOI: https://doi.org/10.1002/advs.201700275 (cit. on p. 14).

[11] A.J. Bard. *Standard Potentials in Aqueous Solution (1st ed.)* Routledge, 1985. DOI: https://doi.org/10.1201/9780203738764 (cit. on p. 14).

[12] Thomas Burdyny and Wilson A. Smith. "CO2 reduction on gas-diffusion electrodes and why catalytic performance must be assessed at commercially-relevant conditions". In: *Energy Environ. Sci.* 12 (5 2019), pp. 1442–1453. DOI: 10.1039/C8EE03134G (cit. on p. 14).

[13] Roger Lin, Jiaxun Guo, Xiaojia Li, Poojan Patel, and Ali Seifitokaldani. "Electrochemical Reactors for CO2 Conversion". In: *Catalysts* 10.5 (2020). ISSN: 2073-4344. DOI: 10.3390/catal10050473 (cit. on p. 15).

[14] B. Zhang et al. M. Liu Y. Pang. "Enhanced electrocatalytic CO2 reduction via field-induced reagent concentration". In: *Nature* 537 (2016), pp. 382–386. DOI: https://doi.org/10.1038/nature19060 (cit. on p. 16).

[15] Tu N. Nguyen and Cao-Thang Dinh. "Gas diffusion electrode design for electrochemical carbon dioxide reduction". In: *Chem. Soc. Rev.* 49 (2020), pp. 7488–7504. DOI: 10.1039/D0CS00230E (cit. on p. 16).

[16] C.Zhang et al. H.Yang Q.Lin. "Carbon dioxide electroreduction on single-atom nickel decorated carbon membranes with industry compatible current densities." In: *Nat. Commun.* 11 (2020). DOI: https://doi.org/10.1038/s41467-020-14402-0 (cit. on p. 16).

[17] Dui Ma, Ting Jin, Keyu Xie, and Haitao Huang. "An overview of flow cell architecture design and optimization for electrochemical CO2 reduction". In: *J. Mater. Chem. A* 9 (37 2021), pp. 20897–20918. DOI: 10.1039/D1TA06101A (cit. on p. 16).

[18] Lorenz M. Baumgartner, Andrey Goryachev, Christel I. Koopman, David Franzen, Barbara Ellendorff, Thomas Turek, and David A. Vermaas. "Electrowetting limits electrochemical CO2 reduction in carbon-free gas diffusion electrodes". In: *Energy Adv.* 2 (11 2023), pp. 1893–1904. DOI: 10.1039/D3YA00285C (cit. on p. 17).

[19] Fabian Bienen et al. "Investigating the electrowetting of silver-based gas-diffusion electrodes during oxygen reduction reaction with electrochemical and optical methods". In: *Electrochemical Science Advances* 3.1 (2023), pp. 210–158 (cit. on p. 17).

[20] Guorui Gao, Cornelius A. Obasanjo, Jackson Crane, and Cao-Thang Dinh. "Comparative analysis of electrolyzers for electrochemical carbon dioxide conversion". In: *Catalysis Today* 423 (2023), p. 114284. ISSN: 0920-5861. DOI: https://doi.org/10.1016/j.cattod.2023.114284 (cit. on p. 18).

[21] Hui-Yun Jeong, Mani Balamurugan, Venkata Surya Kumar Choutipalli, Eun-suk Jeong, Venkatesan Subramanian, Uk Sim, and Ki Tae Nam.

"Achieving highly efficient CO2 to CO electroreduction exceeding 300 mA cm2 with single-atom nickel electrocatalysts". In: *J. Mater. Chem. A* 7 (17 2019), pp. 10651–10661. URL: http://dx.doi.org/10.1039/C9TA02405K (cit. on p. 17).

[22] C.M. Gabardo, C.P. O'Brien, and J.P. Edwards et al. "Continuous carbon dioxide electroreduction to concentrated multi-carbon products using a membrane electrode assembly". In: *Joule* (3 2019), pp. 2777–2791 (cit. on pp. 17, 19).

[23] Alexis T. Bell Lien-Chun Weng and Adam Z.Weber. "Towards membrane-electrode assembly systems for CO2 reduction: a modeling study". In: *Energy Environ. Sci.* 12 (6 2019), pp. 1950–1968. DOI: 10.1039/C9EE00909D (cit. on p. 18).

[24] Lei Ge, Hesamoddin Rabiee, Mengran Li, Siddhartha Subramanian, Yao Zheng, Joong Hee Lee, Thomas Burdyny, and Hao Wang. "Electrochemical CO2 reduction in membrane-electrode assemblies". In: *Chem* 8 (3 Mar. 2022), pp. 663–692. ISSN: 2451-9294. DOI: 10.1016/J.CHEMPR.2021.12.002 (cit. on pp. 18, 33).

[25] H.Yang et al. R.I. Masel Z. Liu. "An industrial perspective on catalysts for low-temperature CO2 electrolysis". In: *Nat. Nanotechnol.* 16 (2021), pp. 118–128. URL: https://doi.org/10.1038/s41565-020-00823-x (cit. on pp. 18, 25).

[26] C. Andronescu D. Segets and U.P. Apfel. "Accelerating CO2 electrochemical conversion towards industrial implementation". In: *Nat Commun* 14 (7950 2023). DOI: https://doi.org/10.1038/s41467-023-43762-6 (cit. on p. 18).

[27] H. Sub K. C. Poon W. Yang Wan and H. Sato. "A review on recent advances in the electrochemical reduction of CO2 to CO with nano-electrocatalysts". In: *RSC Adv 2022* 12 (2022), p. 22703 (cit. on pp. 19, 20).

[28] Sumit Verma, Byoungsu Kim, Huei-Ru "Molly" Jhong, Sichao Ma, and Paul J. A. Kenis. "A Gross-Margin Model for Defining Technoeconomic Benchmarks in the Electroreduction of CO2". In: *ChemSusChem* 9.15 (2016), pp. 1972–1979. DOI: https://doi.org/10.1002/cssc.201600394 (cit. on p. 19).

[29] C.M. Baez-Cotto et al. L. Hu J.A. Wrubel. "A scalable membrane electrode assembly architecture for efficient electrochemical conversion of CO2 to formic acid." In: *Nat. Commun.* 14 (2023), p. 7605. DOI: https://doi.org/10.1038/s41467-023-43409-6 (cit. on p. 19).

[30] Md Golam Kibria, Jonathan P. Edwards, Christine M. Gabardo, Cao-Thang Dinh, Ali Seifitokaldani, David Sinton, and Edward H. Sargent. "Electrochemical CO2 Reduction into Chemical Feedstocks: From Mechanistic Electrocatalysis Models to System Design". In: *Advanced Materials* 31.31 (2019), p. 1807166. DOI: https://doi.org/10.1002/adma.201807166. eprint: https://onlinelibrary.wiley.com/doi/pdf/10.1002/adma.201807166. URL: https://onlinelibrary.wiley.com/doi/abs/10.1002/adma.201807166 (cit. on pp. 19, 20).

[31] Lei Yuan, Shaojuan Zeng, Xiangping Zhang, Xiaoyan Ji, and Suojiang Zhang. "Advances and challenges of electrolyzers for large-scale CO2 electroreduction". In: *Materials Reports: Energy* 3.1 (2023). CO2 Reductions to Fuels and Carbon Feedstocks (Part 1), p. 100177. ISSN: 2666-9358. DOI: https://doi.org/10.1016/j.matre.2023.100177 (cit. on p. 20).

[32] Michael R. Thorson et al. "Effect of Cations on the Electrochemical Conversion of CO2 to CO". In: *J. Electrochem. Soc.* 160 (2013), F69 (cit. on pp. 21, 22).

[33] H. Yu et al Y. Yang Y. Shi. "Mitigating carbonate formation in CO2 electrolysis". In: *Next Energy* 1 (3 2023) (cit. on p. 21).

[34] Tiehuai Li and Minhua Shao. "A minireview on electrochemical CO2 conversion based on carbonate/bicarbonate media". In: *EES. Catal.* 2 (2 2024), pp. 564–572. DOI: 10.1039/D3EY00287J (cit. on p. 21).

[35] Joey Disch, Luca Bohn, Lukas Metzler, and Severin Vierrath. "Strategies for the mitigation of salt precipitation in zero-gap CO2 electrolyzers producing CO". In: *J. Mater. Chem. A* 11 (14 2023), pp. 7344–7357. DOI: 10.1039/D2TA09966G (cit. on p. 22).

[36] Fei-Yue Gao, Rui-Cheng Bao, Min-Rui Gao, and Shu-Hong Yu. "Electrochemical CO2-to-CO conversion: electrocatalysts, electrolytes, and electrolyzers". In: *J. Mater. Chem. A* 8 (31 2020), pp. 15458–15478. DOI: 10.1039/D0TA03525D (cit. on p. 22).

[37] Francois Lapicque, Mariem Belhadj, Caroline Bonnet, Joël Pauchet, and Yohann Thomas. "A critical review on gas diffusion micro and macroporous layers degradations for improved membrane fuel cell durability". In: *Journal of Power Sources* 336 (2016), pp. 40–53. ISSN: 0378-7753. DOI: https://doi.org/10.1016/j.jpowsour.2016.10.037 (cit. on p. 22).

[38] Lien-Chun Weng, Alexis T. Bell, and Adam Z. Weber. "Modeling gas-diffusion electrodes for CO2 reduction". In: *Phys. Chem. Chem. Phys.* 20 (25 2018), pp. 16973–16984. DOI: 10.1039/C8CP01319E. URL: http://dx.doi.org/10.1039/C8CP01319E (cit. on p. 23).

[39] Dunfeng Gao, Pengfei Wei, Hefei Li, Long Lin, Guoxiong Wang, and Xinhe Bao. "Designing Electrolyzers for Electrocatalytic CO2 Reduction". In: *ACTA PHYSICO-CHIMICA SINICA* 37 (May 2021), p. 2009021. DOI: 10.3866/PKU.WHXB202009021 (cit. on p. 23).

[40] et al. Justin C. Bui Eric W. Lees. "Multi-scale physics of bipolar membranes in electrochemical processes". In: *Nature Chem. Eng.* 1 (2024), pp. 45–60. DOI: https://doi.org/10.1038/s44286-023-00009-x (cit. on p. 24).

[41] Ádám Vass, Attila Kormányos, Zsófia Kószó, Balázs Endrődi, and Csaba Janáky. "Anode Catalysts in CO2 Electrolysis: Challenges and Untapped Opportunities". In: *ACS Catalysis* 12.2 (2022), pp. 1037–1051. DOI: 10.1021/acscatal.1c04978 (cit. on pp. 25, 26).

[42] Gede Herry Arum Wijaya, Kwang Seop Im, and Sang Yong Nam. "Advancements in commercial anion exchange membranes: A review of membrane properties in water electrolysis applications". In: *Desalination and*

*Water Treatment* 320 (2024), p. 100605. ISSN: 1944-3986. DOI: https://doi.org/10.1016/j.dwt.2024.100605 (cit. on pp. 25, 42).

[43] H. Wang et al. D. Gao W. Li. "Heterogeneous Catalysis for CO2 Conversion into Chemicals and Fuels." In: *Trans. Tianjin Univ.* 28 (2022), pp. 245–264. DOI: https://doi.org/10.1007/s12209-022-00326-x (cit. on p. 25).

[44] Juan Miguel Álvarez-Gómez and Ana Sofia Varela. "Review on Long-Term Stability of Electrochemical CO2 Reduction". In: *Energy & Fuels* 37.20 (2023), pp. 15283–15308. DOI: 10.1021/acs.energyfuels.3c01847 (cit. on p. 25).

[45] Amin Salehi-Khojin, Huei-Ru Molly Jhong, Brian A. Rosen, Wei Zhu, Sichao Ma, Paul J. A. Kenis, and Richard I. Masel. "Nanoparticle Silver Catalysts That Show Enhanced Activity for Carbon Dioxide Electrolysis". In: *The Journal of Physical Chemistry C* 117.4 (2013), pp. 1627–1632. DOI: 10.1021/jp310509z (cit. on p. 26).

[46] Y. Zhou et al. Q. Lu J. Rosen. "A selective and efficient electrocatalyst for carbon dioxide reduction". In: *Nature* 5 (2014), p. 3242 (cit. on p. 26).

[47] B. Endrődi, G. Bencsik, F. Darvas, R. Jones, K. Rajeshwar, and C. Janáky. "Continuous-flow electroreduction of carbon dioxide". In: *Progress in Energy and Combustion Science* 62 (2017), pp. 133–154. ISSN: 0360-1285. DOI: https://doi.org/10.1016/j.pecs.2017.05.005 (cit. on p. 26).

[48] Siddhartha Subramanian, Kailun Yang, Mengran Li, Mark Sassenburg, Maryam Abdinejad, Erdem Irtem, Joost Middelkoop, and Thomas Burdyny. "Geometric Catalyst Utilization in Zero-Gap CO2 Electrolyzers". In: *ACS Energy Letters* 8.1 (2023), pp. 222–229. DOI: 10.1021/acsenergylett.2c02194 (cit. on p. 27).

[49] Yi Xu, Jonathan P. Edwards, Shijie Liu, Rui Kai Miao, Jianan Erick Huang, Christine M. Gabardo, Colin P. O'Brien, Jun Li, Edward H. Sargent, and David Sinton. "Self-Cleaning CO2 Reduction Systems: Unsteady Electrochemical Forcing Enables Stability". In: *ACS Energy Letters* 6.2 (2021), pp. 809–815. DOI: 10.1021/acsenergylett.0c02401 (cit. on p. 27).

[50] F.F. Klimashin, J. Klusoň, M. Učík, R. Žemlička, M. Jílek, A. Lümkemann, J. Michler, and T.E.J. Edwards. "High-power-density sputtering of industrial-scale targets: Case study of (Al,Cr)N". In: *Materials Design* 237 (2024), p. 112553. ISSN: 0264-1275. DOI: https://doi.org/10.1016/j.matdes.2023.112553 (cit. on p. 29).

[51] C. Gabrielle. *Identification of Electrochemical Processes by Frequency Response Analysis*. Solartron Instrumentation Group, 1980 (cit. on p. 31).

[52] Alexandros Ch. Lazanas and Mamas I. Prodromidis. "Electrochemical Impedance SpectroscopyA Tutorial". In: *ACS Measurement Science Au* 3.3 (2023), pp. 162–193. DOI: 10.1021/acsmeasuresciau.2c00070 (cit. on p. 31).

[53] Roger J. Mortimer. "Spectroelectrochemistry, Methods and Instrumentation". In: *Encyclopedia of Spectroscopy and Spectrometry (Third Edition)*. Ed. by John C. Lindon, George E. Tranter, and David W. Koppenaal.

Third Edition. Oxford: Academic Press, 2017, pp. 172–177. ISBN: 978-0-12-803224-4. DOI: https://doi.org/10.1016/B978-0-12-803224-4.00289-2 (cit. on p. 31).

[54] Bishnu P. Regmi and Masoud Agah. "Micro Gas Chromatography: An Overview of Critical Components and Their Integration". In: *Analytical Chemistry* 90.22 (2018), pp. 13133–13150. DOI: 10.1021/acs.analchem.8b01461 (cit. on p. 31).

[55] M.W. Kanan J.A. Rabinowitz. "The future of low-temperature carbon dioxide electrolysis depends on solving one basic problem." In: *Nat Commun* 11 (2020). ISSN: 5231. DOI: https://doi.org/10.1038/s41467-020-19135-8 (cit. on p. 32).

[56] A. Kukovecz A.A. Samu I. Szenti. "Systematic screening of gas diffusion layers for high performance CO2 electrolysis". In: *Commun Chem* 6 (2023), p. 41. DOI: https://doi.org/10.1038/s42004-023-00836-2 (cit. on pp. 40, 41).

[57] Yen-Chun Chen, Chrysoula Karageorgiou, Jens Eller, Thomas J. Schmidt, and Felix N. Büchi. "Determination of the porosity and its heterogeneity of fuel cell microporous layers by X-ray tomographic microscopy". In: *Journal of Power Sources* 539 (2022), p. 231612. ISSN: 0378-7753. DOI: https://doi.org/10.1016/j.jpowsour.2022.231612 (cit. on p. 41).

[58] Zengcai Liu et al. "CO2 Electrolysis to CO and O2 at High Selectivity, Stability and Efficiency Using Sustainion Membranes". In: *J. Electrochemical Society* 165 (15 2018). DOI: 10.1149/2.0501815jes (cit. on p. 41).

[59] B. Endrődi, E. Kecsenovity, A. Samu, T. Halmágyi, S. Rojas-Carbonell, L. Wang, Y. Yan, and C. Janáky. "High carbonate ion conductance of a robust PiperION membrane allows industrial current density and conversion in a zero-gap carbon dioxide electrolyzer cell". In: *Energy Environ. Sci.* 13 (11 2020), pp. 4098–4105. DOI: 10.1039/D0EE02589E (cit. on p. 42).

[60] Sahil Garg, Carlos A. Giron Rodriguez, Thomas E. Rufford, John R. Varcoe, and Brian Seger. "How membrane characteristics influence the performance of CO2 and CO electrolysis". In: *Energy Environ. Sci.* 15 (11 2022), pp. 4440–4469. DOI: 10.1039/D2EE01818G (cit. on pp. 42, 44).

[61] J. P. Heli et al. G. O. Larrazábal P. Strøm-Hansen. "Analysis of Mass Flows and Membrane Cross-over in CO2 Reduction at High Current Densities in an MEA-Type Electrolyzer". In: *ACS applied materials interfaces* 44 (11 2019), pp. 41281–41288. DOI: https://doi.org/10.1021/acsami.9b13081 (cit. on p. 43).

[62] Kai Han, Ben C. Rowley, Maarten P. Schellekens, Sander Brugman, Michiel P. de Heer, Lucas P. S. Keyzer, and Paul J. Corbett. "Scaling the Electrochemical Conversion of CO2 to CO". In: *ACS Energy Letters* 9.6 (2024), pp. 2800–2806. DOI: 10.1021/acsenergylett.4c00936.

[63] Ralf Krause, David Reinisch, Christian Reller, Helmut Eckert, David Hartmann, Dan Taroata, Kerstin Wiesner-Fleischer, Andreas Bulan, Alexander Lueken, and Guenter Schmid. "Industrial Application Aspects of the Electrochemical Reduction of CO2 to CO in Aqueous Electrolyte". In: *Chemie*

*Ingenieur Technik* 92 (1-2 Jan. 2020), pp. 53–61. ISSN: 1522-2640. DOI: 10.1002/CITE.201900092.

[64] Dezhi Xu, Kangkang Li, Baohua Jia, Wenping Sun, Wei Zhang, Xue Liu, and Tianyi Ma. "Electrocatalytic CO2 reduction towards industrial applications". In: *Carbon Energy* 5.1 (2023), e230. DOI: https://doi.org/10.1002/cey2.230.

[65] Giulia Marcandalli, Mariana C.O. Monteiro, Akansha Goyal, and Marc T.M. Koper. "Electrolyte Effects on CO2Electrochemical Reduction to CO". In: *Accounts of Chemical Research* 55 (14 July 2022), pp. 1900–1911. ISSN: 15204898. DOI: 10.1021/ACS.ACCOUNTS.2C00080. URL: https://doi.org/10.1021/acs.accounts.2c00080.

[66] A. Anzaia A. Yoshizawa M. Higashi and M. Yamauchi. "A membrane electrode assembly-type cell designed for selective CO production from bicarbonate electrolyte and air containing CO2 mixed gas". In: *Energy Adv.* 3 (2024), p. 778.

[67] Shahid Ashraf et al. "Exploring the frontiers of electrochemical CO2 conversion: A comprehensive review". In: *Nano Materials Science* (2024). ISSN: 2589-9651. DOI: https://doi.org/10.1016/j.nanoms.2024.05.005.

[68] Ahmed A.Ali, Harith Mohammed, and Safaa Ahmed. "A Comprehensive Review of the Impact of CO2 Emissions on Global Warming and the Potential Using Solar Energy Mitigation". In: *Al-Rafidain Journal of Engineering Sciences* 2.2 (Sept. 2024), pp. 319–340. DOI: 10.61268/et4axz89.

[69] Adriano Sacco, Roberto Speranza, Umberto Savino, Juqin Zeng, M. Amin Farkhondehfal, Andrea Lamberti, Angelica Chiodoni, and Candido F. Pirri. "An Integrated Device for the Solar-Driven Electrochemical Conversion of CO2 to CO". In: *ACS Sustainable Chemistry & Engineering* 8.20 (2020), pp. 7563–7568. DOI: 10.1021/acssuschemeng.0c02088.

[70] Sandra Hernandez-Aldave and Enrico Andreoli. "Fundamentals of Gas Diffusion Electrodes and Electrolysers for Carbon Dioxide Utilisation: Challenges and Opportunities". In: *Catalysts* 10.6 (2020). ISSN: 2073-4344. DOI: 10.3390/catal10060713.

[71] L. Lin et al. P. Wei H. Li. "CO2 electrolysis at industrial current densities using anion exchange membrane based electrolyzers". In: *Sci. China Chem.* (63 2020), pp. 1711–1715. DOI: https://doi.org/10.1007/s11426-020-9825-9.